UPM report 20221025		
POLITÉCNICA	UPM contribution to Deliverable 5.2 of SANDA project	Date: 25/10/2022
	UPM contribution to D5.2: Report on ESFR, ASTRID and ALFRED sensitivity and impact studies	Pags: 40 Version: 1

SUMMARY

This report contains the UPM contribution to Deliverable 5.2 of the EC SANDA project, Solving Challenges in Nuclear Data for the Safety of European Nuclear facilities (H2020 Grant Agreement number 847552).

MODIFICATIONS TO PREVIOUS VERSION

Written by:	Reviewed by:	Approved by:
Nuria García-Herranz *Antonio Jiménez* *Oscar Cabellos*		

UPM contribution to D5.2: Report on ESFR, ASTRID and ALFRED sensitivity and impact studies

N. García-Herranz, A. Jiménez-Carrascosa, O. Cabellos

Contents

Contents 2
1. Introduction 3
2. Methodology 3
2.1. Methodology for S/U analysis 3
2.2. Processing of JEFF-libraries with AMPX 4
3. Innovative reactor systems under analysis 7
4. Impact studies 11
4.1. Sensitivities 12
4.2. Uncertainties 14
5. Summary and conclusions 20
6. Acknowledgements 20
7. References 20
Annex 1. Biases in sensitivities due to methods and modelling 23
Annex 2. Seven energy groups structure 32
Annex 3. Uncertainty analysis of the partial voiding for the ASTRID-like reactor 33
Annex 4. Sensitivity profiles of critical cross sections 35

1. Introduction

The main purpose of Task 5.1 of SANDA project is to evaluate the impact of (JEFF) nuclear data uncertainties on important design, safety and operational quantities of advanced reactor systems, with the final goal of discussing the implications of the a priori covariance data used and making recommendations about which nuclear data are in need of improvement and what performance gains can be expected as a consequence.

It is well-known that the impact of nuclear data depends on the specific design choices, even within a given "family" of systems. It is therefore essential to consider different systems and to compare the findings when analysing each system individually and jointly.

UPM focuses on neutronic parameters of the following innovative reactors, relying on already-available computational models developed under other EC-funded projects (in parentheses):

- Conceptual sodium-cooled fast reactors (SFR): ASTRID-like (EC FP7 ESNII+ project) and ESFR (EC H2020 ESFR-SMART project)
- Conceptual lead-cooled fast reactors (LFR): ALFRED (EC FP7 ESNII+ project)

SCALE code package [Rearden 2018] is used for the S/U analysis, which has been performed in both 33-energy group and 7-energy group structures. Since impact studies aim at determining the major sources of uncertainty (isotope, reaction and energy group) in order to provide potential evaluation priorities, sensitivities in 7 energy groups (energy bands) together with a JEFF-3.3 covariance matrix in 7 energy groups have been chosen to draw conclusions. The 7-energy group structure is the one proposed by M. Salvatores in NEA/WPEC-SG46 (see Annex 2).

First, a brief description of the employed methodology is given in Section 2. Then, Section 3 includes the performed sensitivity analysis for important key metrics using 3D heterogeneous models. Those models have been preferred to R-Z models taking in consideration the biases in sensitivity coefficients arising from methods and modelling approximations (see Annex 1). In Section 4, uncertainties in the quantities of interest due to JEFF-3.3 nuclear data are compared to the available target accuracies and critical cross sections are identified.

A target accuracy requirement (TAR) assessment, making use of the computed 7-group sensitivities, is being carried out with the aim to find out the required parameter uncertainty reduction so that the integral parameters can fulfil the target accuracies. Results will be reported in Deliverable 5.5 (Report on assessment of nuclear data needs).

2. Methodology

The S/U methodology employed to compute the impact of nuclear data uncertainties is based on the use of TSUNAMI and TSAR modules of the SCALE code package [Rearden 2018]. The processing of JEFF-3.3 nuclear data library for use with TSUNAMI-3D in continuous energy mode has been performed with the AMPX code, also part of the SCALE package [Wiarda 2016].

2.1. Methodology for S/U analysis

TSUNAMI module (*Tools for Sensitivity and Uncertainty Analysis Methodology Implementation*), based on the adjoint-weighted perturbation theory, provides the *sensitivity profiles* (over a range of energy groups) of a model output parameter k to an input parameter α :

$$S_\alpha = \frac{\alpha}{k}\left(\frac{\partial k}{\partial \alpha}\right) \quad (1)$$

For calculating the sensitivity coefficients of the reactivity responses, the SCALE module *Tool for Sensitivity Analysis of Reactivity Responses* (TSAR) is used. From the sensitivity coefficients of the criticality constants

corresponding to two configurations, $S_{\alpha,1}$ and $S_{\alpha,2}$, TSAR computes the relative sensitivity coefficient of the reactivity response as follows:

$$S_{\rho_{1\to2},\alpha} = \frac{\alpha}{|\rho_{1\to2}|}\frac{\partial\rho_{1\to2}}{\partial\alpha} = \frac{\alpha}{|\rho_{1\to2}|}\left(\frac{\partial\lambda_1}{\partial\alpha} - \frac{\partial\lambda_2}{\partial\alpha}\right) = \frac{\lambda_1 S_{\alpha,1} - \lambda_2 S_{\alpha,2}}{|\rho_{1\to2}|} \quad (2)$$

where $\rho_{1\to2}$ denotes the reactivity response and $\lambda = 1/k$.

With the knowledge of the sensitivity profiles S_α and the covariance matrix V_α in a number of energy groups, SCALE performs the uncertainty analysis applying the sandwich rule within SAMS module, the *Sensitivity Analysis Module for SCALE*:

$$\sigma^2 = S_\alpha V_\alpha S_\alpha^T \quad (3)$$

TSUNAMI-3D module provides Monte Carlo-based sensitivities for 3D geometries. It can perform continuous-energy (CE) or multigroup (MG) S/U calculations making use of the 3D Monte Carlo KENO transport code in CE or MG mode respectively.

In the CE approach, sensitivities are computed during a single forward Monte Carlo neutron transport calculation. Two methods are available: the *Iterated Fission Probability* (IFP) methodology and the *Contribution-Linked eigenvalue sensitivity/Uncertainty estimation via Tracklength importance Characterization* (CLUTCH) methodology. The latter is preferred because of its greater computational efficiency and lower memory footprint compared to IFP method.

In the MG approach, sensitivities are computed from one forward and one adjoint transport calculation. The forward and adjoint flux angular moments are tallied at every energy and spatial region.

TSUNAMI-2D module provides deterministic-based sensitivities for 2D X-Y geometries, and it is based on the 2D NEWT transport code[1]. Sensitivities are calculated from one forward and one adjoint transport calculation. The forward and adjoint flux angular moments are determined from the fluxes computed in every quadrature direction, spatial region and energy group.

In this work, MG TSUNAMI-3D has been used to determine the sensitivity profiles of the full 3D heterogeneous models of innovative reactors while CE TSUNAMI-3D y TSUNAMI-2D have been employed for the bias study in Annex 1.

MG TSUNAMI-3D has been chosen as a workable compromise to provide reliable results for 3D heterogenous models due to the following reasons:

1) For full heterogeneous 3D models, CE TSUNAMI-3D demands huge computational requirements (memory, computational time), leading to failure in some cases. This limitation was also observed for Serpent code during the ESFR-SMART project [Margulis 2020].

2) Although CE TSUNAMI-3D is compatible with the use of simplified RZ models, as shown in SANDA-Deliverable D5.1, the bias study performed in Annex 1 shows significant discrepancies in the sensitivities of some reactivity coefficients between 3D heterogeneous and RZ models, suggesting the need of using heterogeneous models to draw reliable conclusions for reactivity parameters.

2.2. Processing of JEFF-libraries with AMPX

As aforementioned, the impact of JEFF-3.3 nuclear data uncertainties [Plompen 2020] on design and safety parameters of advanced nuclear systems is performed with SCALE code package. The use of JEFF nuclear data

[1] NEWT does not solve the transport equation in 2D RZ geometries, so TSUNAMI-2D cannot provide sensitivities for RZ models.

libraries within SCALE system is not straight forward and nuclear data processing must be carried out with the AMPX modular processing code, also part of the SCALE system [Wiarda 2016]. Some efforts have been recently made in this regard. In fact, the processing of JEFF nuclear data libraries with AMPX is being in-depth addressed in the frame of SANDA Task 4.3 and substantial progress have been already made [Jiménez-Carrascosa, 2021a]. Nonetheless, covariance data are also necessary for use with SCALE sensitivity and uncertainty analysis tools. In carrying out this Task 5.1, the JEFF-3.3 covariance matrices have been processed in both 33- and 7-group structures according to the processing route depicted in Figure 1.

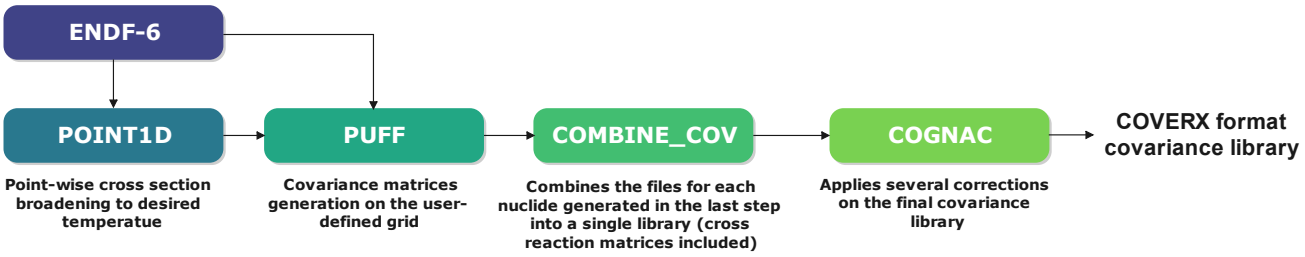

Figure 1. Covariance libraries processing route for AMPX.

The JEFF-3.3 nuclear data library contains 562 nuclides, of which 447 files including covariances. They contain information for the average number of neutrons per fission (File 31), information for the resonance parameters (File 32), information for the neutron cross sections (File 33) and information for exit energy distributions (File 35). PUFF is the main module for the generation of covariance matrices with AMPX with respect to the group-averaged cross section data. A set of files for each nuclide is generated by PUFF and then combined into a single library (including cross reaction and cross material covariance matrices, if available). Finally, several corrections are applied to the library by the COGNAC module solving potential inconsistencies such as a) redundant covariance matrices, b) relative uncertainties larger than 1, c) correlation values with absolute values larger than 1 or d) cross section data without covariance information. Then, a COVERX-formatted library is generated and readable by SCALE modules devoted to S/U analyses.

It is worth mentioning that a weighting spectrum is required for the generation of group-averaged cross section covariances. For that purpose, an optimal function for fast reactor analysis is selected. That function strongly affects to prompt fission neutron spectrum (PFNS) covariances so that the selection of an appropriate weighting spectrum is crucial.

A comprehensive comparison between AMPX and NJOY processing codes is under way in the SANDA Task 4.3 but preliminary analyses have shown a good agreement between both covariance libraries, except for the group containing the threshold for threshold reactions in the 7-group structure. Uncertainty propagation exercises were carried out for the European Sodium Fast Reactor also in the frame of SANDA project [Bécares 2021] showing a good agreement between TSUNAMI-3D and MCNP results. In any case, Figure 2 presents an example concerning covariance processing with AMPX and NJOY. As it can be observed, a very good agreement is obtained in terms of relative standard deviation for both U-238 capture and inelastic scattering reactions.

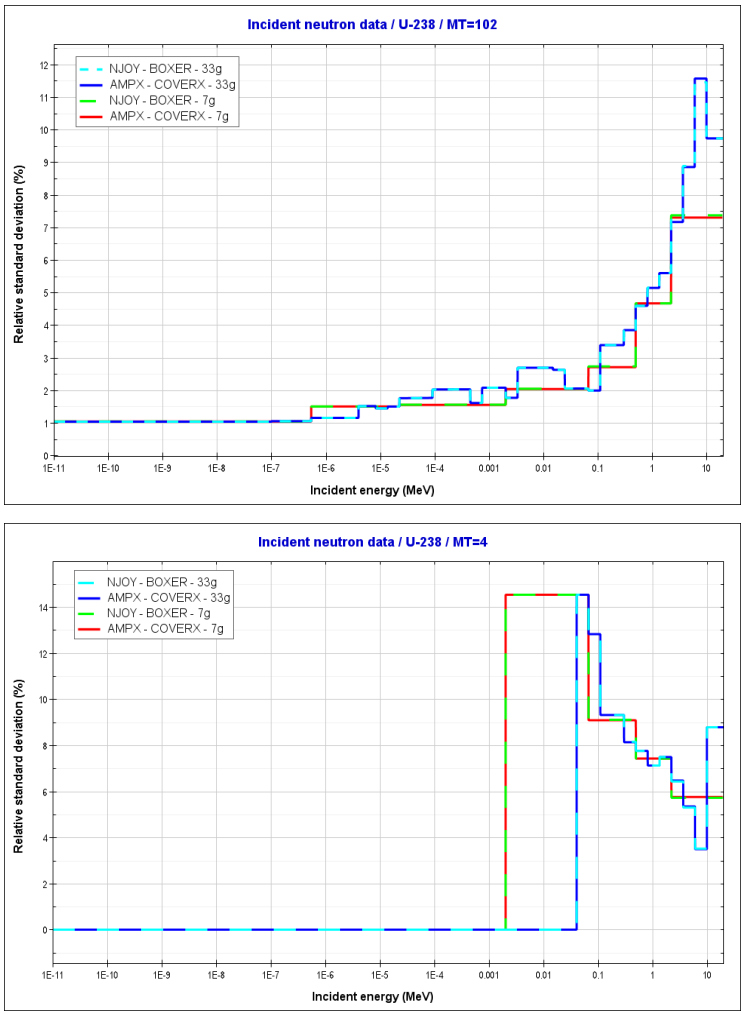

Figure 2. Relative standard deviation for U-238 capture and inelastic scattering collapsed into 7- and 33-energy groups using NJOY2016 and AMPX.

In conclusion, a JEFF-3.3 CE neutron cross section library has been processed with AMPX along with the associated covariance library using different energy group structures. Then, in this work, uncertainty propagation for the considered advanced system is carried out based on both covariance libraries.

3. Innovative reactor systems under analysis

Two SFR designs and one LFR design were selected for the sensitivity and impact studies. Concerning SFR technologies, a commercial-size 3600 MWth core, namely the European Sodium Fast Reactor (ESFR); and a medium-size low-void-effect 1500 MWth core, similar to the Advanced Sodium Technological Reactor for Industrial Demonstration (ASTRID), called ASTRID-like reactor. Concerning LFR technologies, the Advanced Lead-cooled Fast Reactor European Demonstrator (ALFRED), rated 300 MWth, was chosen in this work.

Table 1 compares the design and nominal operation conditions for the three reactors, while Table 2 details the modelling and method used for the sensitivity analysis. Note that the three selected technologies are fast spectrum, mixed-oxide (MOX) fueled reactors.

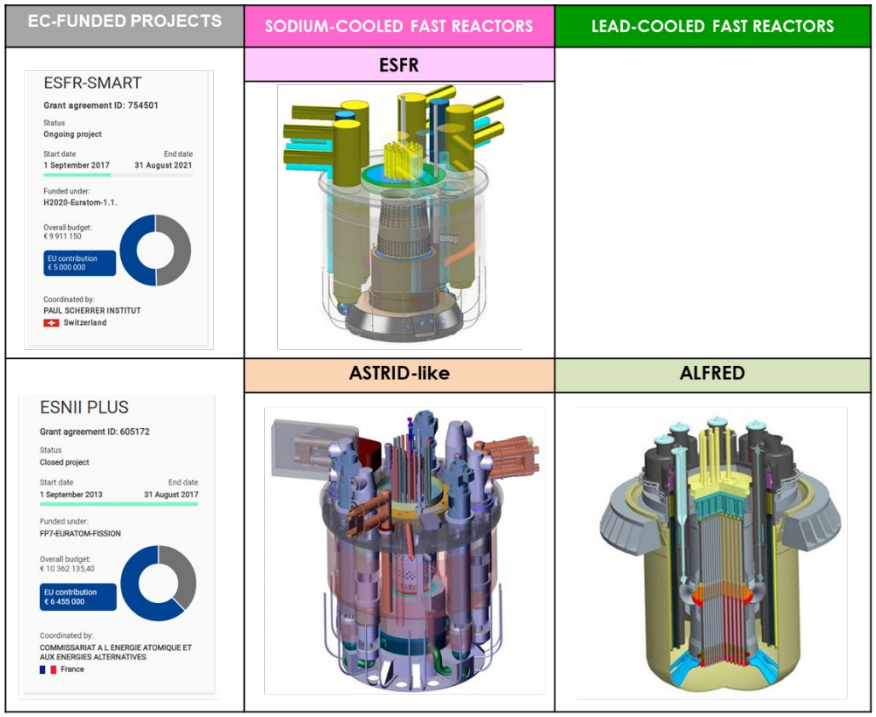

Figure 3. Innovative systems under analysis and related EC-funded projects.

The ESFR core, developed in the Horizon 2020 project ESFR-SMART (2017-2022) [Mikityuk, 2017], is an optimized design of the core proposed within the earlier FP7 CP-ESFR project (2009-2013) [Fiorini 2011]. The core design modifications were aimed at improving the core map symmetry, optimizing the void effect, facilitating the corium relocation toward the corium catcher and achieving low reactivity swing in connection with a flexible breeding and minor actinide burning strategy.

Detailed specifications can be found in [Fridman 2022] and only main characteristics are pointed out here.

The ESFR radial layout is depicted in Figure 4 (left). The active core is composed of hexagonal subassemblies (SA) with a triangular arrangement of 271 pins. It is divided into an inner and an outer fissile fuel region with 216 and 288 SA respectively, both regions loaded with $(U,Pu)O_2$ with a Pu content of 17.99 wt% in the initial core (same initial plutonium content in the whole core). Three rings of radial reflector assemblies (264 SA) surround the active core. In addition, there are two rings for internal spent fuel storage and four rings of shielding (those assemblies were not modelled for neutronic analyses as their neutronic effect is negligible). A total of 31 corium discharge tubes, 24 control and shutdown devices (CSD) and 12 diverse shutdown devices (DSD) complete the core description.

The axial layout is presented in Figure 4 (right). The height of the inner fissile region is shorter than that of the outer fissile region (75 cm versus 95 cm at cold conditions) (the radial power profile is flattened by using different fuel height in inner and outer zones). Fertile blankets are introduced below the inner and outer regions (25 and 5 cm respectively), so that the upper axial fissile boundaries are at the same height for both the inner and outer zones. Above the active core there is a large sodium plenum (60 cm) followed by a neutron absorber. The sodium plenum reflects neutrons down, when liquid, and lets neutrons fly up towards neutron absorber when voided.

The ASTRID-like core was investigated from a neutronic point of view within the EC FP7 ESNII+ project (2013-2017), cross-cutting project supporting the European Sustainable Industrial Initiative [ESNII+ 2013]. It is a medium-size 1500 MWth core with near zero sodium void worth at the End Of Equilibrium Cycle (EOEC) conditions which would prevent and mitigate severe accidents.

Detailed specifications can be found in [Buiron 2019] and only main characteristics are pointed out here.

The ASTRID-like radial layout is depicted in Figure 5 (left). The active core is composed of 291 hexagonal SA with a triangular arrangement of 217 pins. It is divided into an inner and an outer fuel region with 177 and 114 SA respectively, loaded with $(U,Pu)O_2$ with a Pu content of 24.3 wt% and 20.7 wt% respectively in the initial core. Three rings of radial reflector assemblies (216 SA) and four rings of radial shielding assemblies (354 SA) surround the active core. The core is controlled by 12 control and shutdown devices (CSD) and 6 diverse shutdown devices (DSD).

The axial layout in in Figure 5 (right) shows two different heights for the inner and outer fuel zones (60 cm and 90 cm respectively), with an internal axial blanket in the inner region, at the mid-plane in the core (not foreseen in the outer region). There is a thick fertile blanket below the active core. Finally, there is a large sodium plenum (30 cm) on the active core and an absorber shielding at the top, aimed at preventing neutrons from going back to the core during sodium voiding.

The **Advanced Lead-cooled Fast Reactor European Demonstrator (ALFRED)** was chosen in this work as representative of the LFR technology. The considered core design was the one investigated within the EC FP7 ESNII+ project (2013-2017). It is a 300 MWth small-size pool type reactor cooled by pure lead.

The ALFRED radial layout is depicted in Figure 6 (left). The active core is composed of 171 hexagonal subassemblies with a triangular arrangement of 127 pins. It is divided into an inner and an outer fissile fuel region with 57 and 114 SA respectively loaded with $(U,Pu)O_2$ with a higher enrichment in the outer region to flatten the power distribution. Two rings of reflector assemblies surround the active core. The core is controlled by 12 control rods for power regulation and reactivity swing compensation and 4 safety rods for shutdown purposes. The axial layout is depicted in Figure 6 (right).

Detailed specifications can be found in [Grasso 2014]. It is worth it to mention that these core specifications differ from the ones recently presented by ENEA in [Casteluccio 2019] [Casteluccio 2021]; among others, a slightly smaller core is defined (56 and 78 SA loaded in the inner and outer regions respectively).

Table 1. Main nominal parameters for the selected innovative reactors.

	ESFR	ASTRID-like	ALFRED
Thermal power (MWt)	3600	1500	300
Coolant	Sodium	Sodium	Lead
Core inlet/core outlet temperature (ºC)	395/545	400/550	400/480
Average core structure and coolant temperature (ºC)	470	475	440
Average fuel temperature (ºC)	1227	1227	900
Average fertile temperature (ºC)	627	627	-
Fuel type	MOX	MOX	MOX
Pu content at inner/outer zones (wt%)	17.99/17.99	24.3/20.7	21.8/27.9
Number of Subassemblies inner/outer core	216/288	177/114	57/114
Subassembly pitch (cm)	20.99	17.61	17.1
Fissile core diameter D (m) inner/outer zone	3.4 / 5.5	2.7 / 3.8	1.4 / 2.6
Fissile core height H (m) inner/outer zone	0.75 / 0.95	0.60 / 0.90	0.60 / 0.60
Ratio H/D	0.22 / 0.17	0.22 / 0.24	0.87 / 0.47
EALF (MeV)	0.177	0.181	0.123

Table 2. Modelling and methods for sensitivity/uncertainty analysis.

	ESFR	ASTRID-like	ALFRED
Code version	SCALE 6.2.3	SCALE 6.1.3	SCALE 6.1.3
Modelling	3D heterogeneous	3D heterogeneous	3D heterogeneous
Condition	End-of-Cycle	End-of-Cycle	Beginning-of-Cycle
Method	TSUNAMI-3D MG	TSUNAMI-3D MG	TSUNAMI-3D MG
Nuclear data for transport	252g ENDF/B-VII.1	238g ENDF/B-VII.0	238g ENDF/B-VII.0
Covariance data	JEFF-3.3 & ENDF/B-VIII.0-based (56g SCALE6.3beta)		
Integral responses	k-eff Coolant density (full void) Doppler coefficient (±300K) Control rod	k-eff Coolant density (full void)	k-eff Coolant density (-20% inner zone) Doppler coefficient (±300 K)

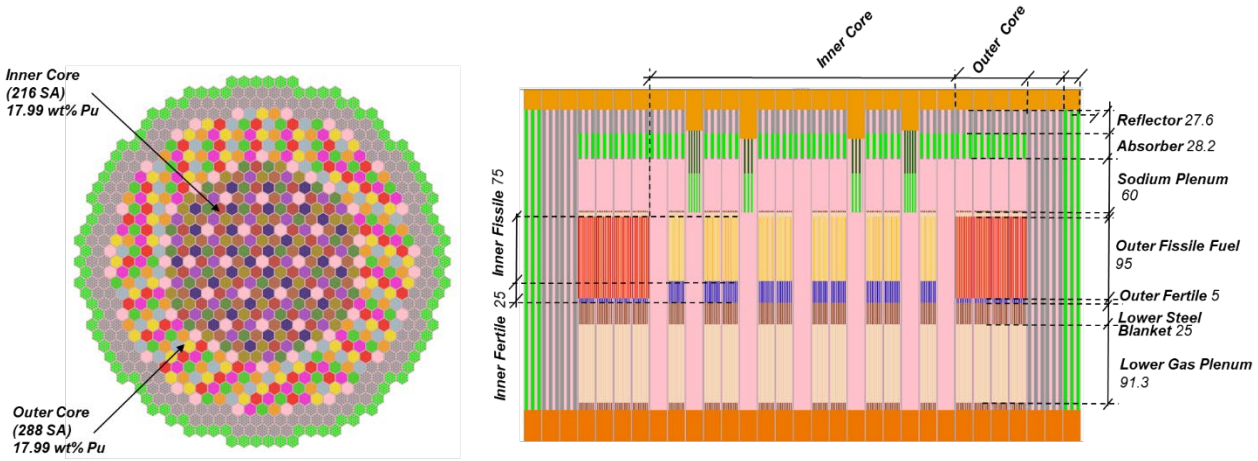

Figure 4. ESFR: developed model for KENO-VI/SCALE.

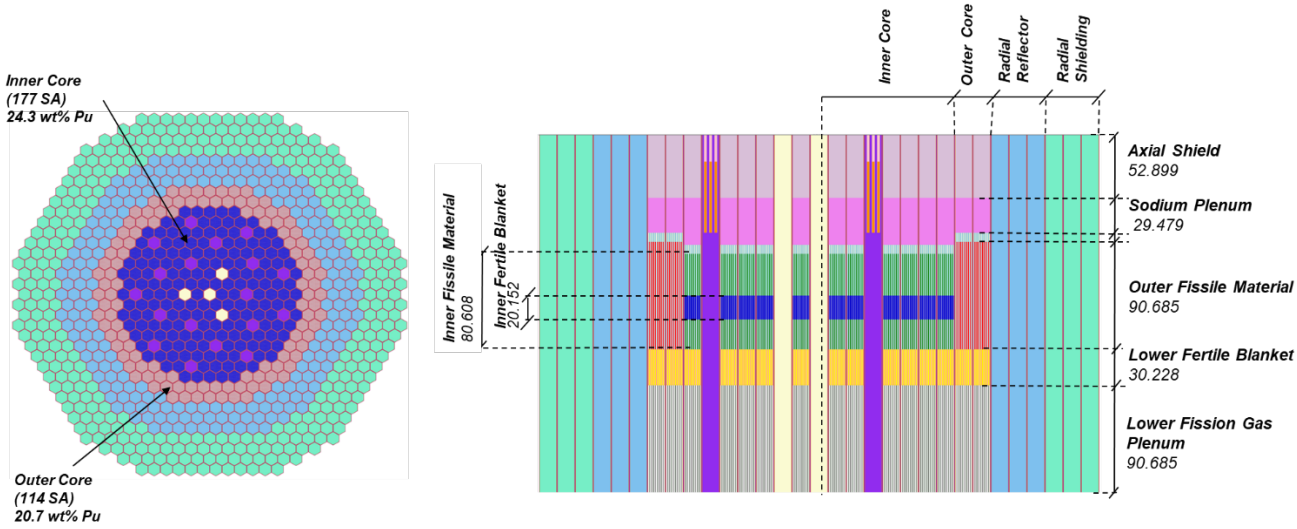

Figure 5. ASTRID-like reactor: developed model for KENO-VI/SCALE.

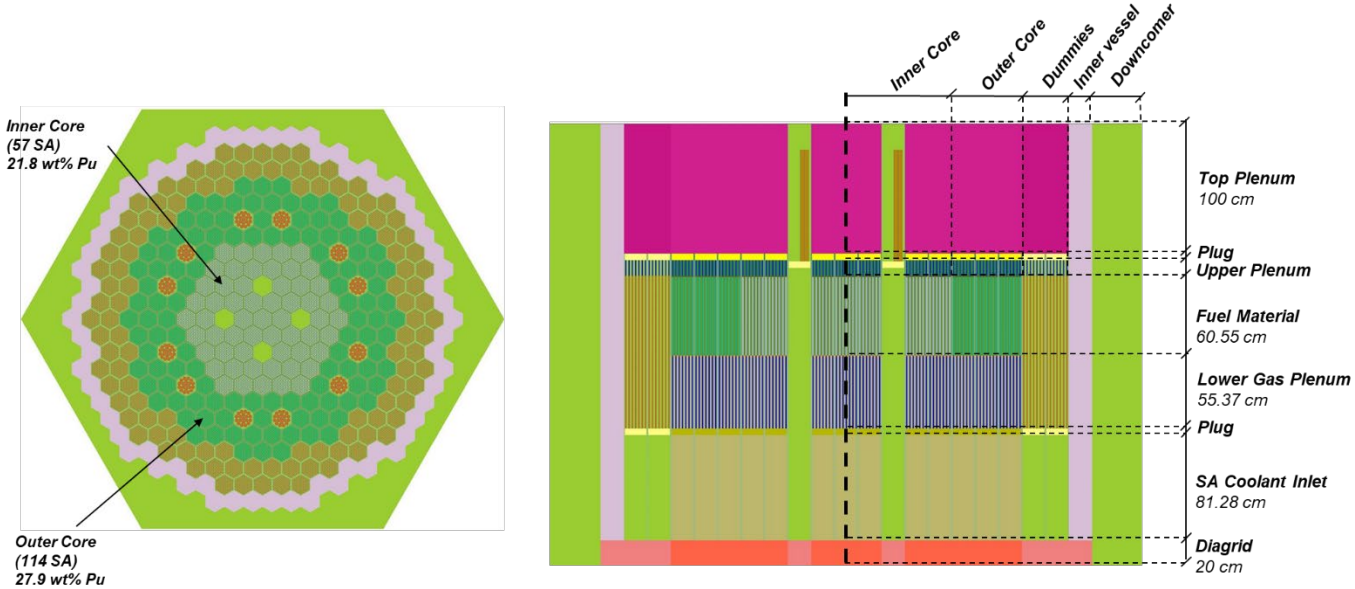

Figure 6. ALFRED: developed model for KENO-VI/SCALE.

4. Impact studies

S/U results for the multiplication factor k_{eff} and reactivity responses of the three advanced systems are jointly presented in order to explore common and different behaviour. Reactivity responses correspond to:

- Fuel Doppler effect. A change of ±300 K from reference fuel temperature (in both inner and outer regions) has been simulated for ESFR and ALFRED. Both scenarios are presented to highlight the different related uncertainties; they are relevant for example for Unprotected Transients of Over-Power (UTOP) or Unprotected Loss Of Off-site Power (ULOOP) [Grasso 2018] respectively.
- Coolant density effect: scenarios in which coolant density decreases with respect to the nominal values by 100% -sodium voiding- in ESFR and ASTRID-like (in both fuel active regions and sodium plenum) and 20% in ALFRED (in inner active region) have been simulated. Moreover, results corresponding to different scenarios of partial voiding are also presented for ASTRID-like in Annex 3.
- Control rods reactivity worth. A perturbed scenario where control rods move from a completely extracted to a completely inserted position is simulated.

The nominal results obtained for the analysed reactor integral responses are presented in Table 3.

Table 3. Nominal values of integral responses.

Reactor	Response	Value ± statistical uncertainty
ESFR	k-eff	1.004992 ± 9 pcm
	Coolant density (full void)	305 ± 12 pcm
	Doppler +300K	-140 ± 11 pcm
	Doppler -300K	177 ± 11 pcm
	Control rod worth	-5028 ± 13 pcm
ASTRID	k-eff	1.00779 ± 8 pcm
	Coolant density (full void)	-536 ± 12 pcm
ALFRED	k-eff	0.99904 ± 10 pcm
	Coolant density (-20% inner region)	193 ± 13 pcm
	Doppler+300K	-112 ± 14 pcm
	Doppler-300K	188 ± 13 pcm

4.1. Sensitivities

The highest integrated sensitivity coefficients (ISC) for the integral responses are given in Tables 4 to 7:

- Sensitivities in k_{eff} are similar for the three reactors. The highest values correspond to Pu isotopes and ^{238}U, being the top sensitivities ^{239}Pu nu-bar and fission and ^{238}U(n, γ); then, nu-bar and fission for ^{238}U, ^{241}Pu and ^{240}Pu. Coolant and structural materials play a less important role, being scattering reactions of ^{56}Fe, ^{16}O, ^{23}Na and Pb isotopes the most significant ones, together with capture reaction of ^{56}Fe.
- Although Doppler sensitivities differ for SFR and LFR reactors, ^{239}Pu and ^{238}U cross sections are very relevant for all scenarios. Doppler effect is more sensitive to ^{238}U (n,n') and ^{238}U (n,γ) following a temperature increase than following a temperature decrease, in which case ^{238}U el. and ^{238}U nubar turn out to be the most relevant ^{238}U reactions. With respect to non-actinide isotopes, elastic scattering cross sections of ^{16}O and ^{56}Fe are significant, although the computed TSUNAMI-3D-based sensitivities exhibit large statistical deviations, being therefore not very reliable.
- Coolant density effect is again very sensitive to ^{239}Pu and ^{238}U cross sections for the three reactors, as well as to elastic scattering of ^{56}Fe. Moreover scattering cross sections of ^{23}Na are relevant for SFR and ^{206}Pb (n,n') for LFR (inelastic scattering of ^{207}Pb and ^{208}Pb are ranked as low as 12th and 16th).
- Control rod worth is very sensitive to the ^{10}B (n,α) cross-section (boron is the absorbing material in the control rods).

Table 4. Reactions with the largest values of the ISC for k_{eff} (top 10 sensitivities together with the largest values corresponding to coolant and structural materials)

ESFR				ASTRID				ALFRED			
	ISC (%/%)		Std. Dev.		ISC (%/%)		Std. Dev.		ISC (%/%)		Std. Dev.
^{239}Pu ν	6.39E-01	±	8.9E-06	^{239}Pu ν	6.71E-01	±	6.9E-06	^{239}Pu ν	6.91E-01	±	1.1E-05
^{239}Pu (n,f)	4.76E-01	±	3.0E-05	^{239}Pu (n,f)	4.90E-01	±	2.9E-05	^{239}Pu (n,f)	4.97E-01	±	3.8E-05
^{238}U (n,γ)	-2.02E-01	±	3.7E-05	^{238}U (n,γ)	-2.01E-01	±	3.1E-05	^{238}U (n,γ)	-1.52E-01	±	3.0E-05
^{238}U ν	1.28E-01	±	4.0E-06	^{238}U ν	1.19E-01	±	2.6E-06	^{241}Pu ν	9.35E-02	±	1.5E-06
^{241}Pu ν	1.01E-01	±	1.5E-06	^{241}Pu ν	9.29E-02	±	1.1E-06	^{238}U ν	8.51E-02	±	3.1E-06
^{240}Pu ν	7.96E-02	±	1.4E-06	^{240}Pu ν	7.30E-02	±	1.0E-06	^{240}Pu ν	8.03E-02	±	1.5E-06
^{238}U (n,f)	7.67E-02	±	1.6E-05	^{238}U (n,f)	7.22E-02	±	1.3E-05	^{241}Pu (n,f)	6.80E-02	±	5.3E-06
^{241}Pu (n,f)	7.60E-02	±	4.9E-06	^{241}Pu (n,f)	6.83E-02	±	4.2E-06	^{240}Pu (n,f)	5.53E-02	±	5.2E-06
^{238}U (n,n')	-7.09E-02	±	1.5E-04	^{238}U (n,n')	-5.88E-02	±	1.1E-04	^{238}U (n,f)	5.22E-02	±	1.2E-05
^{16}O el.	-5.66E-02	±	8.4E-04	^{240}Pu (n,f)	5.03E-02	±	4.3E-06	^{239}Pu (n,γ)	-4.87E-02	±	9.7E-06
^{56}Fe (n,n')	-2.09E-02	±	5.6E-05	^{16}O el.	-4.36E-02	±	7.1E-04	^{208}Pb el.	3.39E-02	±	1.4E-04
^{56}Fe (n,γ)	-1.02E-02	±	2.4E-06	^{56}Fe (n,n')	-1.92E-02	±	5.8E-05	^{207}Pb el.	1.45E-02	±	6.0E-05
^{23}Na (n,n')	-8.43E-03	±	2.7E-05	^{56}Fe (n,γ)	-1.26E-02	±	2.7E-06	^{206}Pb el.	1.39E-02	±	6.0E-05
^{56}Fe el.	6.90E-03	±	3.7E-04	^{56}Fe el.	1.00E-02	±	2.8E-04	^{56}Fe (n,γ)	-1.35E-02	±	2.5E-06
^{52}Cr (n,n')	-4.22E-03	±	8.6E-06	^{23}Na el.	1.02E-02	±	2.9E-04	^{56}Fe (n,n')	-1.29E-02	±	5.3E-05
^{23}Na el.	3.85E-03	±	3.3E-04	^{23}Na (n,n')	-7.18E-03	±	2.4E-05	^{56}Fe el.	8.60E-03	±	2.6E-04

Table 5. Reactions with the largest values of the ISC for Doppler effect (top 10 sensitivities).

	ESFR				ALFRED			
		ISC (%/%)		Std. Dev.		ISC (%/%)		Std. Dev.
Doppler +300K	^{239}Pu (n,f)	7.58E-01	±	3.0E-02 (4%)	^{239}Pu (n,f)	1.15E+00	±	4.9E-02 (4%)
	^{16}O el.	-4.91E-01	±	8.4E-01 (172%)	^{239}Pu ν	6.48E-01	±	1.4E-02 (2%)
	^{238}U (n,n')	-3.86E-01	±	1.6E-01 (41%)	^{238}U (n,n')	-5.83E-01	±	1.8E-01 (30%)
	^{239}Pu ν	3.44E-01	±	8.3E-03 (2%)	^{16}O el.	-5.49E-01	±	1.0E+0 (191%)
	^{56}Na el.	-3.22E-01	±	3.3E-01 (103%)	^{238}U (n,γ)	-4.24E-01	±	3.8E-02 (9%)
	^{239}Pu (n, γ)	3.08E-01	±	8.1E-03 (3%)	^{56}Fe el.	-3.43E-01	±	3.3E-01 (97%)
	^{238}U ν	2.77E-01	±	3.7E-03 (1%)	^{238}U el.	-3.31E-01	±	1.0E-01 (31%)
	^{238}U el.	-2.38E-01	±	1.5E-01 (63%)	^{239}Pu (n, γ)	2.78E-01	±	1.2E-02 (4%)
	^{238}U (n,f)	2.00E-01	±	1.6E-02 (8%)	^{56}Fe (n,n')	-1.93E-01	±	6.7E-02 (34%)
	^{240}Pu ν	1.92E-01	±	1.3E-03 (1%)	^{240}Pu ν	1.65E-01	±	2.0E-03 (1%)
Doppler -300K	^{239}Pu (n,f)	-9.26E-01	±	2.4E-02 (3%)	^{239}Pu (n,f)	-1.11E+00	±	2.9E-02 (3%)
	^{16}O el.	7.17E-01	±	6.7E-01 (93%)	^{16}O el.	7.83E-01	±	6.4E-01 (80%)
	^{239}Pu ν	-5.37E-01	±	6.5E-03 (1%)	^{239}Pu ν	-6.15E-01	±	7.7E-03 (1%)
	^{239}Pu (n, γ)	-2.91E-01	±	6.4E-03 (2%)	^{239}Pu (n, γ)	-3.42E-01	±	7.3E-03 (2%)
	^{56}Na el.	2.88E-01	±	2.6E-01 (92%)	^{238}U el.	2.83E-01	±	6.1E-02 (22%)
	^{238}U ν	-2.51E-01	±	2.9E-03 (1%)	^{238}U ν	-1.92E-01	±	2.2E-03 (1%)
	^{56}Fe el.	2.32E-01	±	2.9E-01 (127%)	^{238}U (n,n')	1.71E-01	±	1.0E-01 (61%)
	^{238}U (n,f)	-2.05E-01	±	1.3E-02 (6%)	^{240}Pu ν	-1.60E-01	±	1.0E-03 (1%)
	^{240}Pu ν	-1.42E-01	±	1.0E-03 (1%)	^{238}U (n,f)	-1.52E-01	±	8.6E-03 (6%)
	^{240}Pu (n,f)	-1.35E-01	±	3.8E-03 (3%)	^{240}Pu (n,f)	-1.43E-01	±	3.9E-03 (3%)

Table 6. Reactions with the largest values of the ISC for coolant density (top 10 sensitivities).

ESFR				ASTRID				ALFRED			
	ISC (%/%)		Std. Dev.		ISC (%/%)		Std. Dev.		ISC (%/%)		Std. Dev.
^{238}U (n,γ)	2.91E+00	±	1.7E-02	^{238}U ν	1.51E+00	±	7.4E-04	^{239}Pu ν	-1.56E+00	±	7.7E-03
^{239}Pu ν	-2.90E+00	±	3.9E-03	^{238}U (n,γ)	1.10E+00	±	7.9E-03	^{239}Pu (n,f)	-1.15E+00	±	2.8E-02
^{56}Fe el.	2.45E+00	±	1.7E-01	^{239}Pu (n,γ)	1.10E+00	±	2.1E-03	^{238}U (n,γ)	8.51E-01	±	2.2E-02
^{239}Pu (n,f)	-1.95E+00	±	1.4E-02	^{56}Fe el.	1.07E+00	±	7.3E-02	^{238}U ν	7.16E-01	±	2.3E-03
^{23}Na (n,n')	1.88E+00	±	1.1E-02	^{238}U (n,f)	9.49E-01	±	3.6E-03	^{238}U (n,n')	-4.74E-01	±	1.0E-01
^{238}U ν	1.70E+00	±	1.7E-03	^{238}U (n,n')	-9.31E-01	±	3.6E-02	^{238}U (n,f)	3.97E-01	±	8.4E-03
^{239}Pu (n,γ)	1.53E+00	±	3.5E-03	^{23}Na (n,n')	8.95E-01	±	5.4E-03	^{206}Pb (n,n')	3.33E-01	±	1.9E-02
^{238}U (n,n')	-1.35E+00	±	7.3E-02	^{23}Na el.	-8.68E-01	±	6.5E-02	^{241}Pu ν	-3.03E-01	±	1.1E-03
^{241}Pu ν	-1.18E+00	±	6.5E-04	^{239}Pu ν	-6.78E-01	±	1.9E-03	^{239}Pu (n,γ)	2.44E-01	±	7.0E-03
^{240}Pu ν	1.00E+00	±	6.0E-04	^{241}Pu ν	-6.02E-01	±	2.9E-04	^{16}O el.	-2.36E-01	±	6.0E-01

Table 7. Reactions with the largest values of the ISC for control rod worth (top 10 sensitivities).

	ESFR		
	ISC (%/%)		Std. Dev.
^{239}Pu (n,f)	4.28E-01	±	8.8E-04
^{239}Pu ν	4.07E-01	±	3.1E-04
^{238}U ν	2.49E-01	±	1.4E-04
^{56}Fe el.	2.45E-01	±	1.1E-02
^{16}O el.	2.41E-01	±	2.4E-02
^{238}U (n,f)	2.01E-01	±	4.8E-04
^{10}B (n,α)	-1.67E-01	±	3.7E-04
^{238}U (n,γ)	1.52E-01	±	1.1E-03
^{240}Pu ν	1.46E-01	±	4.8E-05
^{240}Pu (n,f)	1.28E-01	±	1.4E-04

4.2. Uncertainties

Table 8 shows a summary of the uncertainty quantification analysis for the analysed reactor integral responses using JEFF-3.3 covariances in both 33 and 7 energy groups as well as the state-of-the-art 56g ENDF/B-VIII.0 SCALE covariance matrix. The total uncertainties are compared to the design target accuracies for fast reactors recently updated by the OECD/NEA Working Party on International Nuclear Data Evaluation Co-operation Subgroup 46. The detailed breakdown of uncertainty contributors is shown in Tables 9 to 12.

The uncertainty values (in %) given in Tables 8-12 have two different terms. The first term corresponds to the uncertainty due to nuclear data, and the second term (±) is the term corresponding to the stochastic calculation of sensitivity profiles.

Table 8. Uncertainty quantification results.

Reactor	Response	Target accuracy	Uncertainty [%] 33g Sensitivites 33g JEFF-3.3 COV			Uncertainty [%] 7g Sensitivites 7g JEFF-3.3 COV			Uncertainty [%] 33g Sensitivites 56g ENDF/B-VIII.0 COV		
ESFR	**k-eff**	0.3% = 300 pcm	1.04	±	2.5E-04	0.98	±	4.5E-04	0.90	±	1.0E-04
	Coolant density	5%	25.69	±	1.2E-01	26.86	±	1.7E-01	32.43	±	9.5E-02
	Doppler+300K	5%	4.25	±	5.4E-01	4.16	±	7.6E-01	3.58	±	3.9E-01
	Doppler-300K	5%	4.00	±	5.0E-01	3.63	±	6.5E-01	3.59	±	4.6E-01
	Control	3%	1.96	±	1.1E-02	1.80	±	2.0E-02	1.56	±	7.1E-03
ASTRID	**k-eff**	0.3	0.97	±	2.0E-04	0.92	±	3.6E-04	0.89	±	5.4E-05
	Coolant density	5%	15.78	±	5.2E-02	16.19	±	7.7E-02	18.33	±	3.4E-02
ALFRED	**k-eff**	0.435% = 435 pcm	0.88	±	1.6E-04	0.84	±	3.0E-04	0.85	±	4.7E-05
	Coolant density	5%	6.82	±	2.7E-01	6.42	±	3.6E-01	5.77	±	8.4E-02
	Doppler+300K	5%	6.91	±	6.2E-01	6.55	±	7.8E-01	5.21	±	2.5E-01
	Doppler-300K	5%	3.57	±	3.3E-01	3.46	±	4.8E-01	3.35	±	1.3E-01

Table 9. Detailed breakdown of uncertainty contributors of k_{eff} (contributing more than ~200 pcm for JEFF3.3 COV and top-5 contributors for ENDF/B-VIII.0 COV)

Covariance matrix: 7g JEFF-3.3 COV												
ESFR				**ASTRID**				**ALFRED**				
Reaction	**Δk/k (%)**		**Std. Dev.**	**Reaction**	**Δk/k (%)**		**Std. Dev.**	**Reaction**	**Δk/k (%)**		**Std. Dev.**
^{240}Pu (n,f)	0.57	±	1E-05	^{240}Pu (n,f)	0.50	±	1E-05	^{240}Pu (n,f)	0.55	±	2E-05
^{238}U (n,n')	0.47	±	3E-04	^{238}U (n,n')	0.39	±	2E-04	^{240}Pu (n,f) (n,γ)	-0.41	±	1E-05
^{240}Pu (n,f) (n,γ)	-0.41	±	9E-06	^{240}Pu (n,f) (n,γ)	-0.37	±	7E-06	^{239}Pu ν	0.32	±	1E-06
^{238}U (n,n') (n,f)	-0.34	±	1E-04	^{239}Pu (n,f)	0.34	±	8E-06	^{239}Pu (n,f)	0.32	±	7E-06
^{239}Pu (n,f)	0.33	±	6E-06	^{239}Pu ν	0.31	±	5E-07	^{238}U (n,n')	0.24	±	2E-04
^{239}Pu χ	0.32	±	1E-05	^{238}U (n,n') (n,f)	-0.30	±	8E-05	^{238}U (n,γ)	0.22	±	1E-05
^{238}U (n,n') (n,γ)	0.29	±	2E-04	^{239}Pu χ	0.30	±	8E-06	^{239}Pu χ	0.22	±	9E-06
^{239}Pu ν	0.29	±	6E-07	^{238}U (n,γ)	0.28	±	1E-05	^{238}U (n,n') (n,f)	-0.20	±	6E-05
^{238}U (n,γ)	0.29	±	2E-05	^{238}U (n,n') (n,γ)	0.26	±	2E-04	^{239}Pu (n,f) (n,γ)	0.19	±	5E-06
^{238}U (n,f)	0.20	±	6E-06	^{238}U (n,f)	0.19	±	5E-06	^{240}Pu (n,γ)	0.19	±	5E-06
^{238}U (n,f) (n,γ)	0.19	±	6E-06	^{238}U (n,f) (n,γ)	0.18	±	5E-06	^{238}U (n,n') (n,γ)	0.18	±	2E-04
TOTAL OF LISTED	0.90 (92% TOTAL)			TOTAL OF LISTED	0.83 (91% TOTAL)			TOTAL OF LISTED	0.75 (89% TOTAL)		
TOTAL	**0.98**	**±**	**4E-04**	**TOTAL**	**0.92**	**±**	**4E-04**	**TOTAL**	**0.84**	**±**	**3.0E-04**

Covariance matrix: 56g ENDF/B-VIII.0 COV												
ESFR				**ASTRID**				**ALFRED**				
Reaction	**Δk/k (%)**		**Std. Dev.**	**Reaction**	**Δk/k (%)**		**Std. Dev.**	**Reaction**	**Δk/k (%)**		**Std. Dev.**
^{239}Pu (n,f)	0.56	±	7E-06	^{239}Pu (n,f)	0.58	±	8E-06	^{239}Pu (n,f)	0.59	±	8E-06
^{238}U (n,f) ^{239}Pu (n,f)	0.33	±	3E-06	^{238}U (n,f) ^{239}Pu (n,f)	0.32	±	2E-06	^{238}U (n,f) ^{239}Pu (n,f)	0.28	±	2E-06
^{238}U (n, γ)	0.25	±	7E-06	^{239}Pu (n, γ)	0.25	±	8E-06	^{239}Pu (n, γ)	0.27	±	1E-05
^{238}U (n, n')	0.24	±	6E-05	^{238}U (n, γ)	0.25	±	6E-06	^{238}U (n, γ)	0.19	±	5E-06
^{239}Pu (n, γ)	0.22	±	7E-06	^{238}U (n, n')	0.20	±	4E-05	^{239}Pu ν	0.19	±	2E-07
TOTAL OF LISTED	0.77 (85% TOTAL)			TOTAL OF LISTED	0.77 (87% TOTAL)			TOTAL OF LISTED	0.75 (88% TOTAL)		
TOTAL	**0.90**	**±**	**7E-05**	**TOTAL**	**0.89**	**±**	**5E-05**	**TOTAL**	**0.85**	**±**	**5E-05**

Table 10. Detailed breakdown of uncertainty contributors of Doppler effect (top-5 contributors).

	Covariance matrix: 7g JEFF-3.3 COV							
	ESFR				ALFRED			
	Reaction	% Δρ/ρ		Std. Dev.	Reaction	% Δρ/ρ		Std. Dev.
Doppler +300K	^{238}U (n,n')	2.75	±	6E-01	^{238}U (n,n')	4.20	±	7E-01
	^{238}U el. (n,n')	1.74	±	2E-01	^{238}U el. (n,n')	2.45	±	2E-01
	^{240}Pu (n,f)	1.68	±	9E-03	^{206}Pb (n,n')	2.12	±	1E-01
	^{238}U (n,n') (n, f)	-1.36	±	7E-02	^{238}U (n,n') (n, γ)	1.76	±	9E-02
	^{239}Pu (n, γ)	1.35	±	9E-03	^{240}Pu (n,f)	1.56	±	7E-03
	TOTAL OF LISTED	3.66 (88% TOTAL)			TOTAL OF LISTED	5.80 (89% TOTAL)		
	TOTAL	**4.16**	**±**	**8E-01**	**TOTAL**	**6.55**	**±**	**8E-01**
Doppler -300K	^{240}Pu (n,f)	1.44	±	7E-03	^{16}O el.	1.56	±	4E-01
	^{56}Fe el.	1.43	±	4E-01	^{240}Pu (n,f)	1.51	±	8E-03
	^{16}O el.	1.41	±	4E-01	^{239}Pu (n, γ)	1.32	±	8E-03
	^{239}Pu χ	1.21	±	8E-03	^{238}U (n,n')	1.24	±	2E-01
	^{239}Pu (n, γ)	1.21	±	7E-03	^{238}U el. (n,n')	1.20	±	1E-01
	TOTAL OF LISTED	3.01 (83% TOTAL)			TOTAL OF LISTED	3.07 (89% TOTAL)		
	TOTAL	**3.63**	**±**	**7E-01**	**TOTAL**	**3.46**	**±**	**5E-01**

	Covariance matrix: 56g ENDF/B-VIII.0 COV							
	ESFR				ALFRED			
	Reaction	% Δρ/ρ		Std. Dev.	Reaction	% Δρ/ρ		Std. Dev.
Doppler +300K	^{239}Pu (n,f)	1.69	±	7E-03	^{238}U (n,n')	2.12	±	2E-01
	^{239}Pu (n, γ)	1.60	±	1E-02	^{239}Pu (n,f)	2.05	±	7E-03
	^{23}Na el.	1.48	±	4E-01	^{207}Pb (n,n')	1.73	±	3E-02
	^{238}U (n,n')	1.35	±	8E-02	^{239}Pu (n,n')	1.58	±	5E-02
	^{238}U (n,f) ^{239}Pu (n,f)	0.68	±	2E-03	^{239}Pu χ	1.41	±	2E-03
	TOTAL OF LISTED	3.14 (88% TOTAL)			TOTAL OF LISTED	4.02 (77% TOTAL)		
	TOTAL	**3.58**	**±**	**4E-01**	**TOTAL**	**5.21**	**±**	**2E-01**
Doppler -300K	^{23}Na el.	1.59	±	4E-01	^{239}Pu (n, γ)	1.91	±	1E-02
	^{239}Pu (n, γ)	1.54	±	9E-03	^{239}Pu (n,f)	1.57	±	4E-03
	^{239}Pu (n,f)	1.51	±	4E-03	^{238}U (n,n')	1.03	±	8E-02
	^{54}Fe el.	1.17	±	2E-01	^{52}Cr el.	0.79	±	3E-02
	^{238}U (n,n')	1.08	±	2E-01	^{238}U (n,f) ^{239}Pu (n,f)	0.71	±	1E-03
	TOTAL OF LISTED	3.13 (87% TOTAL)			TOTAL OF LISTED	2.88 (86% TOTAL)		
	TOTAL	**3.59**	**±**	**5E-01**	**TOTAL**	**3.35**	**±**	**1E-01**

Table 11. Detailed breakdown of uncertainty contributors on coolant density effect (contributing more than ~2% pcm for JEFF3.3 COV and top-5 contributors for ENDF/B-VIII.0 COV)

Covariance matrix: 7g JEFF-3.3 COV												
ESFR				**ASTRID**				**ALFRED**				
Reaction	**% Δρ/ρ**		**Std. Dev.**	**Reaction**	**% Δρ/ρ**		**Std. Dev.**	**Reaction**	**% Δρ/ρ**		**Std. Dev.**	
^{239}Pu (n,f)	19.77	±	7E-03	^{239}Pu (n,f)	11.5	±	5E-03	^{206}Pb (n,n')	4.58	±	1E-01	
^{239}Pu (n,γ)	9.05	±	3E-03	^{239}Pu (n,γ)	6.34	±	3E-03	^{238}U (n,n')	3.18	±	2E-01	
^{238}U (n,n')	8.85	±	1E-01	^{238}U (n,n')	6.07	±	6E-02	^{207}Pb (n,n')	2.38	±	4E-02	
^{56}Fe el.	7.25	±	1E-01	^{238}U (n,n') (n,f)	-4.46	±	2E-02	^{238}U (n,n') (n,f)	2.17	±	7E-02	
^{239}Pu (n,f) (n, γ)	-6.93	±	1E-03	^{239}Pu (n,f) (n, γ)	-4.39	±	9E-04	^{238}U (n,n') (n,γ)	1.97	±	1E-01	
^{23}Na (n,γ)	6.31	±	3E-04	^{238}U (n,γ)	3.75	±	1E-03	^{239}Pu (n,f)	1.54	±	4E-03	
^{238}U (n,γ)	6.10	±	2E-03	^{23}Na (n,γ)	3.70	±	2E-04	^{208}Pb (n,n')	1.33	±	3E-02	
^{238}U (n,n') (n,f)	-5.60	±	2E-02	^{240}Pu (n,f)	3.23	±	2E-03					
^{241}Pu (n,f)	5.44	±	7E-04	^{56}Fe el.	3.10	±	4E-02					
^{238}U el. (n,n')	-5.23	±	3E-02	^{238}U el. (n,n')	-3.08	±	2E-02					
^{240}Pu (n,f)	4.61	±	3E-03	^{241}Pu (n,f)	2.65	±	4E-04					
^{23}Na (n,n')	4.41	±	3E-03	^{238}U (n,f)	2.54	±	1E-03					
^{238}U (n,n') (n,γ)	-4.20	±	2E-02	^{240}Pu (n,f) (n, γ)	2.42	±	1E-03					
^{240}Pu (n,f) (n, γ)	3.35	±	2E-03	^{238}U (n,f) (n, γ)	2.26	±	9E-04					
^{238}U el. (n,f)	2.87	±	1E-02	^{238}U (n,n') (n,γ)	-2.18	±	2E-02					
^{56}Fe (n,γ)	2.86	±	8E-04	^{56}Fe (n,γ)	2.16	±	8E-04					
^{238}U el. (n, γ)	2.69	±	4E-03	^{23}Na (n,n')	2.09	±	1E-03					
^{238}U (n,f)	2.65	±	1E-03	^{238}U el. (n,f)	2.02	±	9E-03					
^{23}Na el.	2.64	±	4E-02	^{239}Pu χ	1.85	±	7E-04					
^{238}U (n,f) (n, γ)	2.53	±	1E-03	^{23}Na el.	1.71	±	1E-02					
TOTAL OF LISTED	26.12 (97% TOTAL)			TOTAL OF LISTED	15.71 (97% TOTAL)			TOTAL OF LISTED	5.69 (89% TOTAL)			
TOTAL	26.86	**±**	**2E-01**	**TOTAL**	16.19	**±**	**8E-02**	**TOTAL**	**6.42**	**±**	**4E-01**	

Covariance matrix: 56g ENDF/B-VIII.0 COV												
ESFR				**ASTRID**				**ALFRED**				
Reaction	**% Δρ/ρ**		**Std. Dev.**	**Reaction**	**% Δρ/ρ**		**Std. Dev.**	**Reaction**	**% Δρ/ρ**		**Std. Dev.**	
^{23}Na (n,n')	20.32	±	1E-02	^{239}Pu (n,f)	11.8	±	4E-03	^{207}Pb (n,n')	2.60	±	2E-02	
^{239}Pu (n,f)	19.73	±	6E-03	^{23}Na (n,n')	9.8	±	7E-03	^{206}Pb (n,n')	2.58	±	2E-02	
^{239}Pu (n,γ)	9.09	±	3E-03	^{239}Pu (n,γ)	6.43	±	2E-03	^{208}Pb (n,n')	1.83	±	4E-02	
^{23}Na el.	6.89	±	9E-02	^{239}Pu (n,f) (n, γ)	-3.42	±	4E-04	^{239}Pu (n,f)	1.67	±	5E-03	
^{239}Pu (n,f) (n, γ)	-5.42	±	7E-04	^{238}U (n,n')	3.15	±	9E-03	^{238}U (n,n')	1.43	±	5E-02	
TOTAL OF LISTED	30.05 (93% TOTAL)			TOTAL OF LISTED	16.62 (91% TOTAL)			TOTAL OF LISTED	4.66 (81% TOTAL)			
TOTAL	**32.43**	**±**	**1E-01**	**TOTAL**	**18.33**	**±**	**3E-02**	**TOTAL**	**5.77**	**±**	**8E-02**	

Table 12. Detailed breakdown of uncertainty contributors of control rod worth (top-5 contributors).

Covariance matrix: 7g JEFF-3.3 COV			
ESFR			
Reaction	% Δρ/ρ		Std. Dev.
^{240}Pu (n,f)	1.09	±	5E-04
^{56}Fe el.	0.85	±	2E-02
^{238}U (n,f)	0.52	±	3E-04
^{238}U (n,n') (n,f)	-0.49	±	4E-03
^{239}Pu χ	0.48	±	3E-04

Covariance matrix: 56g ENDF/B-VIII.0 COV			
ESFR			
Reaction	% Δρ/ρ		Std. Dev.
^{239}Pu (n,f)	0.73	±	2E-04
^{23}Na el.	0.57	±	6E-03
^{238}U (n,f).^{239}Pu (n,f)	0.50	±	8E-05
^{56}Fe el.	0.40	±	2E-03
^{54}Fe el.	0.35	±	3E-03

The uncertainty analysis shows:

- Recent covariance evaluations (JEFF-3.3 and ENDF/B-VIII.0-based) predict more similar global uncertainties in the integral parameters than previous evaluations used to. This is due to compensation effects as individual contributions differ significantly.
- Using JEFF-3.3 **the major contributors to k_{eff} uncertainties** for the three reactors are the same actinides: ^{240}Pu, ^{239}Pu and ^{238}U. In order to meet the k_{eff} target accuracies for the three reactors, it is imperative to reduce the uncertainty in the reactions contributing with more than ~300 pcm:
  - ^{240}Pu (n,f) (this reaction is not a major contributor when using ENDF/B-VIII.0 covariances)
  - ^{238}U (n,n') and ^{238}U (n,γ)
  - ^{239}Pu ν, ^{239}Pu (n,f) and ^{239}Pu χ
  - Good correlated data between fission and capture of ^{240}Pu, ^{240}Pu (n,f) (n,γ), as well as between fission and inelastic of ^{238}U, ^{238}U (n,f) (n,n'), are needed because of the significant impact of the energy correlation of those cross-sections on the uncertainty estimation.
  - It is worth it to mention that the covariance term ^{238}U (n,f) ^{239}Pu (n,f) has a strong impact in the global uncertainty when using ENDF/B-VIII.0 covariances.
- Using JEFF-3.3, **the major contributors to Doppler uncertainties** differ significantly between SFR and LFR. The uncertainty in the Doppler effect for LFR following a temperature increase exceeds the target accuracy (assuming it is 5%) while the accuracy is not exceeded following a temperature decrease. The main contributor is ^{238}U (n,n'), which is responsible of 64% of the global uncertainty in the parameter, followed by the covariance terms ^{238}U el.(n,n') and ^{238}U (n, γ)(n,n') and by ^{206}Pb (n,n'). Since sensitivity of Doppler effect to ^{238}U (n,n') is less important in SFR, its contribution to Doppler uncertainty is not so relevant. When using ENDF/B-VIII.0 the uncertainty is dominated by capture and fission of ^{239}Pu, being

conclusions in agreement with [Casteluccio 2021]. In summary, Doppler S/U analysis leads to include the following cross-sections contributing to uncertainty more than ~2% in the potential list for uncertainty reduction:

- ^{206}Pb (n,n')
- Correlated data ^{238}U el. (n,n') and ^{238}U (n,n') (n, γ)

- Using JEFF-3.3, **the uncertainty in sodium voiding for SFR** by far exceeds the target accuracy (assuming it is 5%). Main contributors are ^{239}Pu (fission and capture) and ^{238}U cross sections. Fission of ^{240}Pu and ^{241}Pu also play a role. Regarding non-actinide isotopes, ^{56}Fe contributes via capture and elastic scattering and ^{23}Na mainly via capture. Inelastic and elastic scattering of ^{23}Na are ranked as low as 13rd and 23rd respectively, being their contribution much higher when using ENDF/B-VIII.0 covariances (ranked 1st and 4th respectively).

  It is worth it to mention that those conclusions correspond to a full voiding. The partial-voiding analysis performed for ASTRID-like reactor in Annex 3 shows that target accuracies are also exceeded when voiding only inner or outer fissile regions, while the lowest uncertainties correspond to the plenum voiding. The relative importance of major contributors changes among the different scenarios: when voiding plenum regions, elastic scattering of ^{56}Fe and ^{23}Na are the most important contributors; when voiding fuel regions, particularly the outer fuel zone, inelastic scattering of ^{23}Na becomes more relevant.

- Using JEFF-3.3, **the uncertainty in the cooling density effect for LFR** exceeds the target accuracy (assuming it is 5%) mainly due to inelastic scattering of ^{206}Pb, ^{207}Pb and ^{238}U. The contribution of inelastic scattering of ^{208}Pb is much lower than when using ENDF/B-VIII.0 covariances. However, in case of coolant density reduction in the outer zone, the contributor's importance changes, similarly to ASTRID.

  To cover all the possible scenarios, coolant density analysis leads to include the following cross-sections, contributing to uncertainty more than ~2%, in the potential list for uncertainty reduction:

  - ^{239}Pu (n,γ) and good correlated data with fission: ^{239}Pu (n, γ) (n,f)
  - ^{238}U (n,f) and good correlated data with capture and elastic: ^{238}U (n,f) (n, γ) and ^{238}U el. (n,f)
  - ^{23}Na (n,γ), elastic and inelastic
  - ^{26}Fe elastic and (n, γ)
  - Inelastic scattering of lead isotopes, ^{206}Pb, ^{207}Pb, ^{208}Pb

- Using JEFF-3.3, **the uncertainty in the control rod worth** does not exceed the target accuracy (assuming it is 5%), so no additional uncertainty reduction would be required.

- Scattering reactions play a very relevant role in most examined reactivity effects. There is a significant sensitivity to the angular distribution of the neutrons scattered in these fast spectrum systems (especially after sodium voiding, as shown in Annex 2 for the ASTRID-like reactor). However, the impact of the covariances in the angular distribution of scattering data has not been considered, which could significantly affect uncertainty results, as shown in [Hill and Jeong 2017] [Fiorito 2019]. Consequently, an identified gap in this study is the lack of consideration of covariances in angular scattering distributions.

5. Summary and conclusions

The impact of nuclear data on parameters of ESFR, ASTRID-like and ALFRED advanced reactors has allowed the identification of the nuclear data in need of improvement. Recommendations about which energy groups should have the highest priority for the uncertainty reduction will be given in Deliverable 5.5. As future work, a TAR assessment will be carried out to identify the required uncertainty reduction so that the integral parameters can fulfil the target accuracies. It is important to mention that the three selected technologies are fast spectrum, mixed-oxide (MOX) fueled reactors; conclusions for other compositions, such as metallic fuels, could differ.

An identified gap in this study is the lack of consideration of covariances in angular scattering distributions. Due to the importance of scattering reactions in most examined reactivity effects, that aspect should receive more attention, together with the large statistical deviations accompanying scattering reaction sensitivities.

The impact studies have been performed using MG TSUNAMI-3D methodology and 3D heterogeneous models of the reactors (instead of RZ models). A bias analysis in sensitivity coefficients arising from nuclear data, methods and modelling approximations has shown that:

- The use of different nuclear data libraries barely impacts sensitivities, although the application to other advanced systems could lead to different results.
- RZ models are good enough for the sensitivity analysis of multiplication factors, but do not provide reasonable results for some reactivity parameters.
- MG TSUNAMI-3D method provides consistent sensitivities with respect to CE TSUNAMI-3D except for elastic scattering reactions, which are affected by high statistical uncertainties in both methodologies. A comparison against deterministic-based sensitivities provided by TSUNAMI-2D is under way.

6. Acknowledgements

SCALE6.3 beta version has been provided by Oak Ridge National Laboratory. The ESFR model has been obtained through the HORIZON2020 EU ESFR-SMART project (number 754501), while ASTRID-like and ALFRED models through the 7th FP EU ESNII plus project (number 605172).

7. References

[Aliberti 2011] G. Aliberti *et al., Impact on sensitivity coefficients of typical approximations used in scoping sensitivity analysis*, In Proc. Int. Conf. on Mathematics and Computational Methods applied to Nuclear Science and Engineering, Rio de Janeiro (Brazil) May 8-12, 2011.

[Bécares 2021] V. Bécares *et al*., *Comparison of Sensitivity/Uncertainty analysis methodologies in the European Sodium Fast Reactor*, In Proc. Spanish Nuclear Society Annual Meeting, Granada (Spain) 6-8 October, 2021.

[Bostelmann 2020] F. Bostelmann, *Systematic Sensitivity and Uncertainty Analysis of Sodium-cooled Fast Reactors Systems*. PhD dissertation, École Polytechnique Fédérale de Laussane, Switzerland (2020).

[Buiron 2019] Buiron L., Sciora P., Rimpault G., Additional ASTRID benchmark, WPRS SFR UAM, July 2019

[ESNIIplus 2013] EC Community Research and Development Information Service – ESNII plus project. https://cordis.europa.eu/project/id/605172

[Fiorini 2011] G.L. Fiorini and A. Vasile, *European Commission – 7th Framework Programme: The Collaborative Project on European Sodium Fast Reactor (CP ESFR), Nucl. Eng. Des., vol. 241, no. 9, pp. 3461–3469, Sep. 2011*

[Fridman 2022] E. Fridman et al., Neutronic analysis of the European Sodium Fast Reactor: Part I - fresh core result. Journal of Nuclear Engineering and Radiation Science 8(1) (2022), 011301.

[Grasso 2014] G. Grasso et al. The core design of ALFRED, a demonstrator for the European lead-cooled reactors. Nuclear Engineering and Design 278 (2014) 287–301

[Grasso 2018] G. Grasso et al. Stress-testing the ALFRED design - Part I: Impact of Nuclear Data Uncertainties on Design Extension Conditions Transients. Prog. Nucl. Energ. 106 (2018) 372-386

[Casteluccio 2019] D.M. Castelluccio, F. Lodi, V.G. Peluso and G. Grasso, Preliminary evaluation of ALFRED S/U analysis, Meeting of the OECD/NEA-NSC-WPEC-SG46, 25-26 November 2019

[Casteluccio 2021] D.M. Castelluccio, G. Grasso, F. Lodi, V.G. Peluso and A. Mengoni, Nuclear data target accuracy requirements for advanced reactores: The ALFRED case, Annals of Nuclear Energy 162 (2021)

[Fiorito 2019] L. Fiorito, J. Dyrda, M. Fleming, JEFF-3.3 covariance application to ICSBEP using SANDY and NDAST, EPJ Web of Conferences 211, 07003 (2019)

[Hill and Jeong 2017] I. Hill, S. Jeong, Status and analysis of P1 angular scattering sensitivity data available with the database for ICSBEP (DICE). M&C 2017, Jeju, Korea, April 16-20

[Jiménez-Carrascosa 2020] A. Jiménez-Carrascosa *et al.*, *Joint UPM and CIEMAT contribution: Progress on ESFR*, WPEC Subgroup 46 (SG46) WebEx meeting, 11 November 2020 (https://www.oecd-nea.org/download/wpec/sg46/meetings/2020-11/)

[Jiménez-Carrascosa 2021a] A. Jiménez-Carrascosa *et al*., *Processing of JEFF nuclear data libraries for the SCALE Code System and testing with criticality experiments*, In Proc. Spanish Nuclear Society Annual Meeting, Granada (Spain), October 6-8, 2021.

[Jiménez-Carrascosa 2021b] A. Jiménez-Carrascosa *et al., Nuclear data sensitivity and uncertainty analysis for reactor physics parameters of the European Sodium Fast Reactor*, In Proc. European Nuclear Young Generation Forum, Tarragona (Spain), September 27-30, 2021.

[Margulis 2020] M. Margulis et al., Analysis of safety and performance parameters of the ESFR-SMART core at end of cycle, Deliverable D1.2.2 ESFR-SMART project, Grant Agreement No. 754501.

[Mikityuk 2017] K. Mikityuk *et al.*, *ESFR-SMART: New Horizon-2020 Project on SFR Safety*. AQ6 474 Proc. IAEA FR2017, Ekaterinburg (Russian Federation).

[OECD/NEA 2017] *Efficient and Effective Use of Integral Experiments for Nuclear Data Validation*. OECD/NEA WPEC Subgroup 46, https://www.oecd-nea.org/download/wpec/sg46/ (2017).

[Perfetti 2017] C. M. Perfetti *et al.*, *SCALE Continuous-Energy Eigenvalue Sensitivity Coefficient Calculations*. Nuclear Science and Engineering 182 (2016) 332-353.

[Plompen 2020] A. J. M. Plompen *et al*., *The joint evaluated fission and fusion nuclear data library, JEFF-3.3*. European Physical Journal A 56 (2020) 181.

[Rearden 2011] B. T. Rearden *et al.*, *Sensitivity and Uncertainty Analysis Capabilities and Data in SCALE*. Nuclear Technology 174 (2011) 236-288.

[Rearden 2018] B. T. Rearden and M. A. Jessee (Eds.), *SCALE Code System*. Oak Ridge National Laboratory report ORNL/TM-2005/39 Version 6.2.3 (2018).

[Rineiski 2022] A. Rineiski *et al*., *ESFR-SMART core safety measures and their preliminary assessment*. Journal of Nuclear Engineering and Radiation Science 8(1) (2022), 011322.

[Romojaro 2015] P. Romojaro *et al., D10.1 Report on sensitivity analysis of MYRRHA with list of key reactions*. CHANDA project Deliverable (2015).

[Romojaro 2019] P. Romojaro *et al.*, *Sensitivity methods for effective delayed neutron fraction and neutron generation time with SUMMON*. Annals of Nuclear Energy 126 (2019) 410–418.

[Romojaro 2021] P. Romojaro *et al.*, *On the importance of target accuracy assessments and data assimilation for the co-development of nuclear data and fast reactors: MYRRHA and ESFR*. Annals of Nuclear Energy 161 (2021) 1-13.

[Wiarda 2016] D. Wiarda *et al.*, *AMPX-6: A Modular Code System for Processing ENDF/B*. Oak Ridge National Laboratory report ORNL/TM-2016/43 (2016).

Annex 1. Biases in sensitivities due to methods and modelling

In this section, the biases in TSUNAMI-based sensitivity coefficients arising from methods and modelling assumptions have been evaluated. Not only sensitivities for the multiplication factor but also for safety-relevant reactivity responses have been analysed. In the study, propagated uncertainties are also included for the considered parameters to illustrate the impact of the sensitivity profiles on the final uncertainty.

Assuming linearity, the TSUNAMI-based sensitivity profiles will have biases and uncertainties due to:

- **Nuclear data:** uncertainties in nuclear data or the use of different evaluated data libraries can impact the sensitivity profiles.
- **Methods:** if CE TSUNAMI-3D approach is used, it can be assumed that statistical uncertainty is the only source of uncertainty, which can be made acceptably small by running more histories (the largest statistical errors appear for scattering reactions). Other sources of errors, such as biases from numerical algorithms, are negligible, as demonstrated in D5.1 where a good agreement with the sensitivities provided by other methodologies (i.e. MCNP/KSEN) was shown.

  On the other hand, if MG TSUNAMI-3D approach is applied, apart from the statistical uncertainty there will also be errors due to the self-shielding approximations for the multigroup cross sections. It is relevant to quantify those systematic errors to verify if they may be judged as negligible or may require consider some conservative bias. Moreover, the method employed to compute the forward and adjoint angular flux moments could also impact the results.

  If TSUNAMI-2D approach is employed, biases in sensitivities will come from the different approximations involved in deterministic methods: self-shielding approximations for the multigroup cross sections, space-energy-direction discretization, truncated expansions of angular functions. Nevertheless, sensitivities will not be affected by statistical errors.
- **Modelling:** models used in the calculation of sensitivity profiles for reactors do not usually correspond to the real detailed 3D systems, which would require huge computational resources (memory and computational time). Instead, simplifications such as homogenizing regions or development of RZ models are usually carried out. The bias in the computed sensitivities due to the modelling must be addressed.

Firstly, the biases arising from the use of different nuclear data libraries have been assessed via the intercomparison of sensitivity profiles obtained for the considered system using both ENDF/B-VII.1 and JEFF-3.3 nuclear data libraries. Then, TSUNAMI-3D CE and MG approaches have been compared. Finally, the most common simplification regarding modelling strategies has been studied, concluding the suitability of simplified models for obtaining sensitivity coefficients. Concerning uncertainty propagation, the 56-group covariance data from SCALE6.2, which is mostly based on ENDF/B-VII.1 data, is applied.

1. Models and selected parameters

Since the study is focused on the performance of sensitivity analysis methodologies for advanced nuclear systems, a simplified supercell model has been selected (Figure 13). The model has been created as a simplification of the commercial-size European Sodium Fast Reactor (ESFR) core [Rineiski 2022]. That design has been proposed and analysed in the frame of the ESFR-SMART project. This simplified model consists of a central control assembly surrounded by 16 MOX-fueled hexagonal sub-assemblies. The fuel sub-assemblies correspond to the inner fuel region of the core at Beginning-of-Life (BOL), preserving the axial heterogeneity. That is, the model includes the sodium plenum above the active part, which allows to simulate different sodium void scenarios (i.e., fissile region, sodium plenum, full void). In addition, this model also enables the characterization of the control rod worth through the insertion of the Control and Shutdown Device (CSD). Geometrical and material specifications can be extracted from [Fridman 2022].

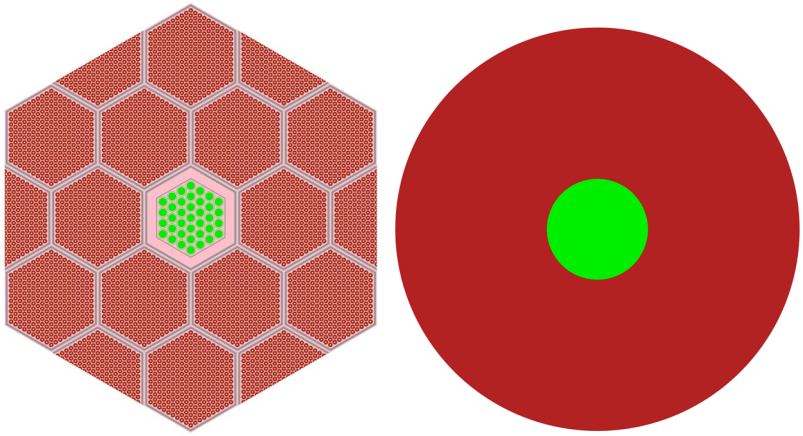

Figure A1.1. Heterogeneous and homogenized MOX-fueld sodium fast reactor supercell model.

The model presented in Figure A1.1 (left) is referred as heterogeneous model hereinafter since a homogeneous RZ model is also included in the study. In the latter case, the model consists of two equivalent concentric cylinders, as shown in Figure A1.1 (right), with radius determined to preserve the total mass of each material in the different regions. This simplified RZ model allows to evaluate a quite common assumption in scoping sensitivity coefficients since computational codes may be unable to deal with large heterogeneous cores.

Table A1.I collects all the cases included in the analysis, that will allow to evaluate three different sources of biases on sensitivity coefficients: a) the impact of using different nuclear data libraries (ENDF/B-VII.1 and JEFF-3.3), b) the impact of the employed methodology (TSUNAMI-3D CE and MG), and c) the effect of geometry modelling (heterogeneous and homogeneous models).

Table A1.1. Models and parameters evaluated.

Methodology	Model	Library	Parameters
TSUNAMI-3D CE	Heterogeneous	ENDF/B-VII.1	Multiplication factor Sodium void worth (3 cases) Control rod worth
TSUNAMI-3D CE	Homogeneous	ENDF/B-VII.1	Multiplication factor Sodium void worth (3 cases) Control rod worth
TSUNAMI-3D MG	Heterogeneous	ENDF/B-VII.1	Multiplication factor Sodium void worth (1 case)
TSUNAMI-3D CE	Heterogeneous	JEFF-3.3	Multiplication factor

As first exercise, an intercomparison of different existing sensitivity methodologies was carried out in the frame of the SANDA project [Bécares 2021]. Three different Monte Carlo neutron transport codes, including TSUNAMI-3D CE, were applied to the sensitivity analysis of the same system, the ESFR core. Sensitivity coefficients provided by TSUNAMI-3D CE showed a good agreement compared to MCNP for both the multiplication factor and the selected sodium void reactivity worth. Nonetheless, remarkable inconsistencies were observed when dealing with scattering reactions, since associated sensitivity coefficients present notable statistical dispersion. In this work, since a more simplified system is selected, significant efforts are devoted to the proper convergence of sensitivities for the scattering reactions.

2. Intercomparison results: impact of nuclear data libraries on sensitivity coefficients

As aforementioned, the first source of bias in sensitivities is associated to nuclear data. In previous projects [Romojaro 2015], these biases were characterized using MCNP6.1.1b and both JEFF-3.1.2 and ENDF/B-VII.0 nuclear data libraries for the critical configuration of the Lead-cooled Fast Reactor MYRRHA. In general, a very good agreement was observed between sensitivities with both libraries for the major contributors. Some deviations were found for specific quantities such as Pu-239 ν, Pu-239 capture, Pu-240 ν, Pu-239 fission, Pu-238 fission, U-238 capture, U-238 elastic and Fe-56 capture within specific energy ranges.

This exercise is reevaluated here for the supercell model using TSUNAMI-3D CE and both ENDF/B-VII.1 and JEFF-3.3. It is worth mentioning that the JEFF-3.3 library has been processed with the AMPX code using the latest updates in SCALE6.3β11 version as reported in [Jiménez-Carrascosa 2021a].

Results of the criticality calculations are presented in Table A1.2. As a result of applying different nuclear data libraries, a deviation of around 400 pcm can be found for the multiplication factor. Integrated sensitivity coefficients are depicted in Figure A1.2 along with their ratio.

Table A1.2. TSUNAMI-3D CE multiplication factor results for the supercell using different nuclear data libraries.

Library	Mutliplication factor	Δk_{eff} (pcm)	$\Delta k_{eff}/k_{eff}$ (%)
ENDF/B-VII.1	1.05257 ± 0.00009	(ref)	1.417
JEFF-3.3	1.05665 ± 0.00009	408	1.460

As it can be observed, both libraries provide similar values for the major sensitivity coefficients since deviations are lower than 2% except for the following reactions: U-238 capture, O-16 elastic, Pu-239 capture, Pu-240 capture and Fe-56 inelastic. Both scattering reactions present deviations of around 7.1% and the corresponding sensitivity profiles are presented in Figure A1.3, where statistical uncertainties are also plotted, being negligible. Scattering reactions with lower k-eff sensitivity coefficients also exhibit significant deviations (~22% for U-238 elastic). Those reactions may play a more important role for reactivity effects.

The uncertainty propagation from both sensitivity profiles is carried out using the SCALE6.2-56g covariance data and results are included in Table A1.2. For this system, the nuclear data-induced uncertainty in the multiplication factor is around 1420 pcm and the use of different nuclear data libraries on the sensitivity analysis leads to a deviation of 40 pcm in the overall uncertainty. It is worth mentioning that the partial contribution of several quantities to the overall uncertainty may change depending on the applied sensitivity profile as depicted in Table A1.3. For instance, the contribution of the uncertainty due to U-238 inelastic-elastic is 0.23% when using ENDF/B-VII.1-based sensitivities while its contribution is around 0.42% if JEFF-3.3 sensitivities are applied. Then, despite of the fact that the overall uncertainty is quite similar independently on the nuclear data library employed on scoping sensitivities, special attention should be paid to specific contributors. Thus, it is recommendable to perform cross-comparison exercises based on the same nuclear data library and the associated covariance library.

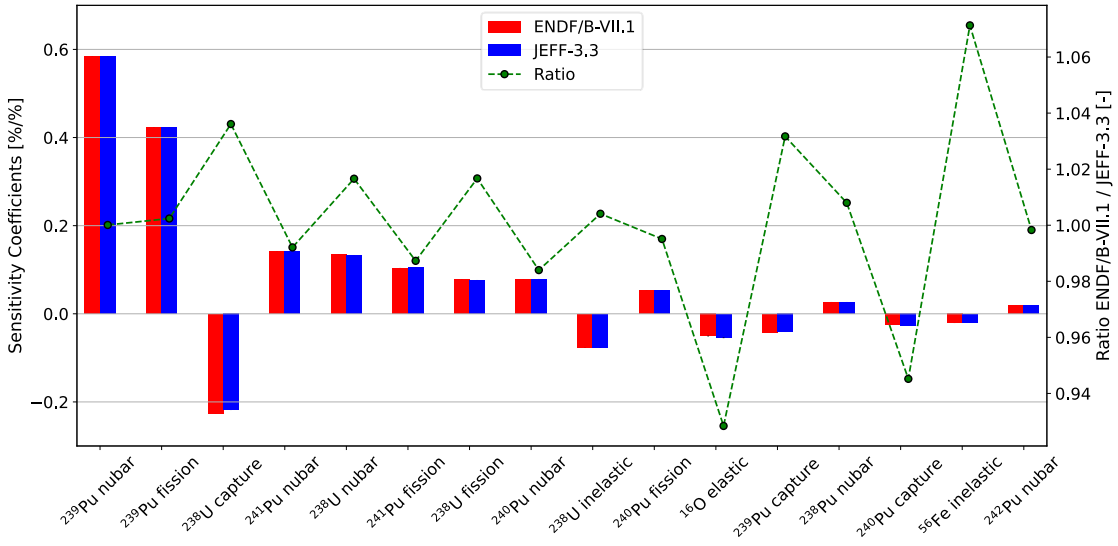

Figure A1.2. Top 16 integrated multiplication factor sensitivity coefficients for the supercell determined with TSUNAMI-3D CE using different nuclear data libraries.

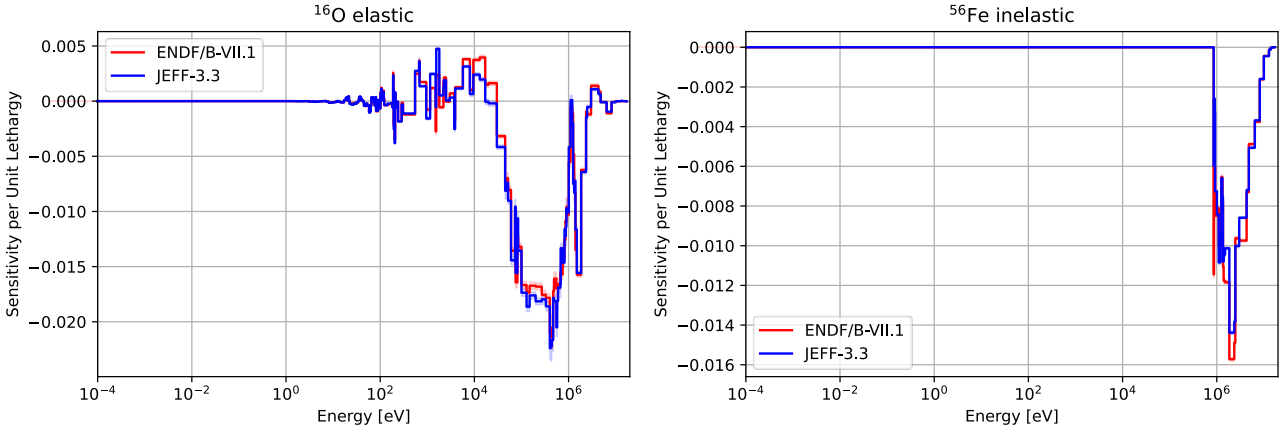

Figure A1.3. Multiplication factor sensitivity profiles of the O-16 elastic and Fe-56 inelastic for both ENDF/B-VII.1 and JEFF-3.3 nuclear data libraries.

Table A1.3. Detailed breakdown of uncertainty contributors for multiplication factor using different nuclear data libraries and 56-group SCALE6.2 covariance matrix.

TSUNAMI-3D CE: ENDF/B-VII.1				TSUNAMI-3D CE: JEFF-3.3			
	% Δk/k		Std. Dev.		% Δk/k		Std. Dev.
^{238}U (n,n')	1.23	±	6E-04	^{238}U (n,n')	1.24	±	7E-04
^{238}U (n,γ)	0.30	±	4E-06	^{238}U (n,n')-(n,n)	0.42	±	6E-04
^{241}Pu χ	0.24	±	9E-05	^{238}U (n,γ)	0.29	±	4E-06
^{238}U (n,n')-(n,n)	0.23	±	7E-04	^{241}Pu χ	0.24	±	9E-05
^{239}Pu (n,γ)	0.22	±	2E-06	^{239}Pu (n,γ)	0.20	±	2E-06

3. Intercomparison results: impact of CE and MG approaches on sensitivity coefficients

In this section, TSUNAMI-3D CE and MG methodologies are evaluated on the supercell model. Initially, TSUNAMI-3D MG predicted a multiplication factor of around 500 pcm higher than TSUNAMI-3D CE. Nonetheless, an improved self-shielding description was applied for the fuel pins adjacent to the subassembly wrapper as suggested in [Bostelmann 2020]. This modification has reduced the difference up to 100 pcm, which is a significant improvement. However, the impact of that modification appears to be practically negligible in sensitivity coefficients.

Multiplication factor sensitivity coefficients for the supercell model are depicted in Figure A1.4. TSUNAMI-3D MG generally provides very similar results compared to TSUNAMI-3D CE. The most relevant differences are associated to U-238 inelastic, O-16 elastic and Fe-56 inelastic, being negligible the associated statistical errors in both calculations. Nonetheless, propagated total uncertainties are very similar as presented in Table A1.4 and a good agreement is observed on the uncertainty breakdown (see Table A1.5). Thus, multiplication factor sensitivities obtained with TSUNAMI-3D MG will perfectly capture the system behaviour.

Additionally, a sodium void scenario has been studied using both methodologies. Sodium void worth values obtained with TSUNAMI-3D CE and MG are very similar, with a difference of about 15 pcm. Sensitivities associated to the reactivity response present dramatic deviations for elastic and inelastic scattering reactions, which are moreover accompanied by large statistical errors.

The behaviour exhibited by scattering reactions requires further research in order to determine the origin of the discrepancies between methodologies.

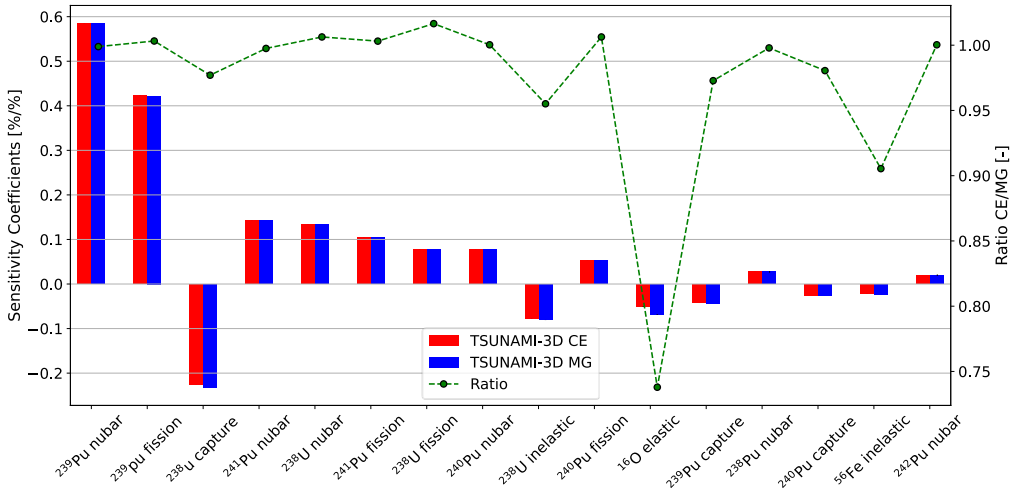

Figure A1.4. Top 16 integrated multiplication factor sensitivity coefficients determined with TSUNAMI-3D CE and TSUNAMI-3D MG for the heterogenous 3D model.

Table A1.4. Multiplication factor uncertainty determined with TSUNAMI-3D CE and MG.

Parameter	TSUNAMI-3D CE	TSUNAMI-3D MG
Multiplication factor	1.417%	1.441%

Table A1.5. Detailed breakdown of uncertainty contributors for multiplication factor using different methodologies and 56-group SCALE6.2 covariance matrix.

TSUNAMI-3D CE				TSUNAMI-3D MG			
	% Δk/k		Std. Dev.		% Δk/k		Std. Dev.
^{238}U (n,n')	1.23	±	6E-04	^{238}U (n,n')	1.27	±	6E-04
^{238}U (n,γ)	0.30	±	4E-06	^{238}U (n,γ)	0.31	±	8E-06
^{241}Pu χ	0.24	±	9E-05	^{241}Pu χ	0.24	±	2E-06
^{238}U (n,n')-(n,n)	0.23	±	7E-04	^{239}Pu (n,γ)	0.22	±	6E-06
^{239}Pu (n,γ)	0.22	±	2E-06	^{239}Pu χ	0.19	±	1E-06

4. Intercomparison results: impact of modelling approaches on sensitivity coefficients

As previously introduced, a quite common assumption for sensitivity analysis is to adopt simplified models, which require lower computational resources. For example, RZ models are being systematically employed for TAR analyses within the NEA WPEC/SG46 [OECD/NEA 2017]. In this section, an evaluation of the impact due to the RZ modelling is carried out for five different parameters are evaluated in this exercise: the multiplication factor, the control rod reactivity worth and three sodium void scenarios.

Control rod is basically represented as a cylinder homogenizing absorbing and structural materials. This simplification will modify the reactivity coefficient since absorption effects are unrealistically amplified as concluded in [Aliberti 2011]. Additionally, due to the homogenization process, sodium void scenarios will not be equivalent between both models. That is, in the 3D model, sodium void effects are simulated by removing the sodium coolant within the subassembly wrapper. On the other hand, in RZ geometry, sodium is completely removed in a homogenized region. This will lead to an amplification of the sodium void worth when working with simplified models.

The calculated parameters obtained with TSUNAMI-3D CE for both models are compared in Table A1.6. It can be observed that the use of a RZ model leads to a change of 274 pcm in the multiplication factor, while reactivity effects are much more different, providing the RZ model unrealistic results.

Firstly, multiplication factor sensitivities calculated with both models are presented in Figure A1.5. In general, a good agreement is found between both models. However, remarkable deviations are obtained mainly for structural materials: O-16 elastic, Fe-56 inelastic and Fe-56 capture with deviation of around 3%, 10% and 5% respectively. These results are consistent with other previous studies [Jiménez-Carrascosa 2021b, Aliberti 2011] and it can be concluded that RZ models are suitable for multiplication factor sensitivity analyses. In fact, uncertainties in multiplication factor for both models are practically similar as it can be observed in Table A1.7.

Table A1.6. Supercell parameters evaluated with 3D and RZ geometry models.

Parameter	Heterogenous 3D model	Homogeneous RZ model	Δρ (pcm)
Multiplication factor	1.05257 ± 0.00009	1.05531 ± 0.00008	274
Control rod worth	-4959 ± 11	-5914 ± 11	-955
Na void: fissile region	1294 ± 11	1800 ± 11	507
Na void: plenum region	-1566 ± 12	-954 ± 11	621
Na void: full void	-410 ± 11	762 ± 11	1172

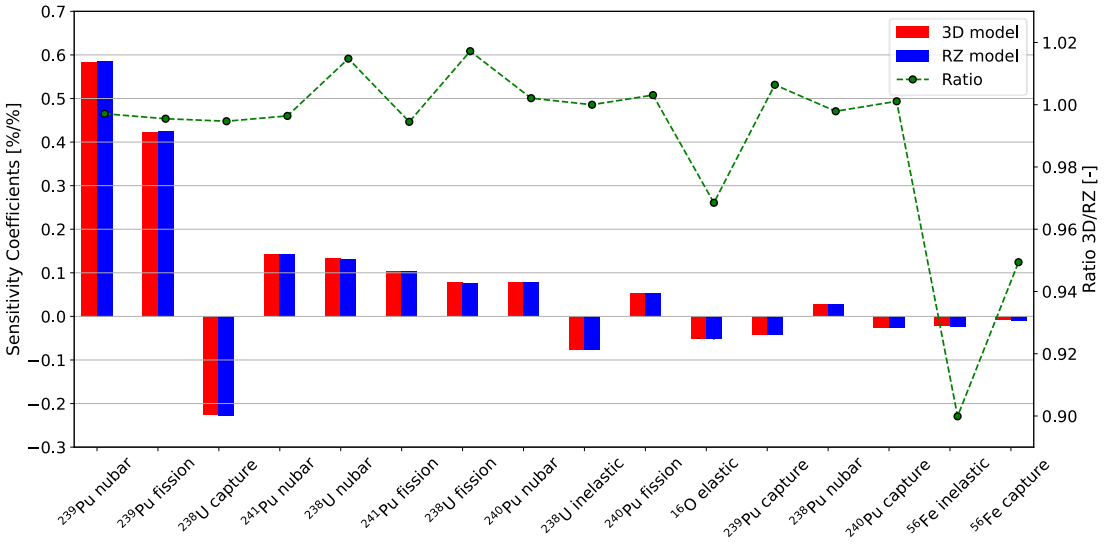

Figure A1.5. Top 16 integrated multiplication factor sensitivity coefficients determined with TSUNAMI-3D CE for the heterogeneous 3D and RZ simplified models.

Table A1.7. Multiplication factor and reactivity effects uncertainty determined with TSUNAMI-3D CE.

Parameter	Heterogenous 3D model	Homogeneous RZ model
Multiplication factor	1.417%	1.412%
Control rod worth	2.642%	2.818%
Na void: fissile region	7.420%	6.680%
Na void: plenum region	3.747%	5.390%
Na void: full void	32.620%	18.418%

Control rod worth sensitivities computed for both models are compared in Figure A1.6. Although in previous works [Aliberti 2011] it was concluded that simplified models are not adequate for control rod worth sensitivity analyses, this study, with the latest sensitivity methodologies, shows a quite good agreement. Most significant deviations are associated to B-10 (n,α), U-238 capture, U-238 inelastic, Fe-56 inelastic and elastic scattering and Pu-239 capture.

Propagated uncertainties in control rod worth are also included in Table A1.7, with a deviation of around 0.2% between both models. In general, major contributors to the total uncertainty present a good agreement (see Table A1.8), but U-238 elastic-inelastic component should be highlighted since its contribution is 0.12% higher in the RZ model.

Table A1.8. Detailed breakdown of uncertainty contributors for control rod worth using the heterogeneous 3D and RZ simplified models. and 56-group SCALE6.2 covariance matrix.

Heterogeneous 3D model				Homogeneous RZ model			
	% Δρ/ρ		Std. Dev.		% Δρ/ρ		Std. Dev.
^{238}U (n,n')	2.35	±	2E-02	^{238}U (n,n')	2.45	±	2E-02
^{238}U χ	0.62	±	3E-03	^{238}U χ	0.59	±	2E-03
^{241}Pu χ	0.43	±	2E-03	^{238}U (n,n')-(n,n)	0.48	±	2E-02
^{239}Pu χ	0.38	±	1E-03	^{241}Pu χ	0.43	±	2E-03
^{238}U (n,n')-(n,n)	-0.36	±	2E-02	^{56}Fe elastic	0.42	±	3E-03

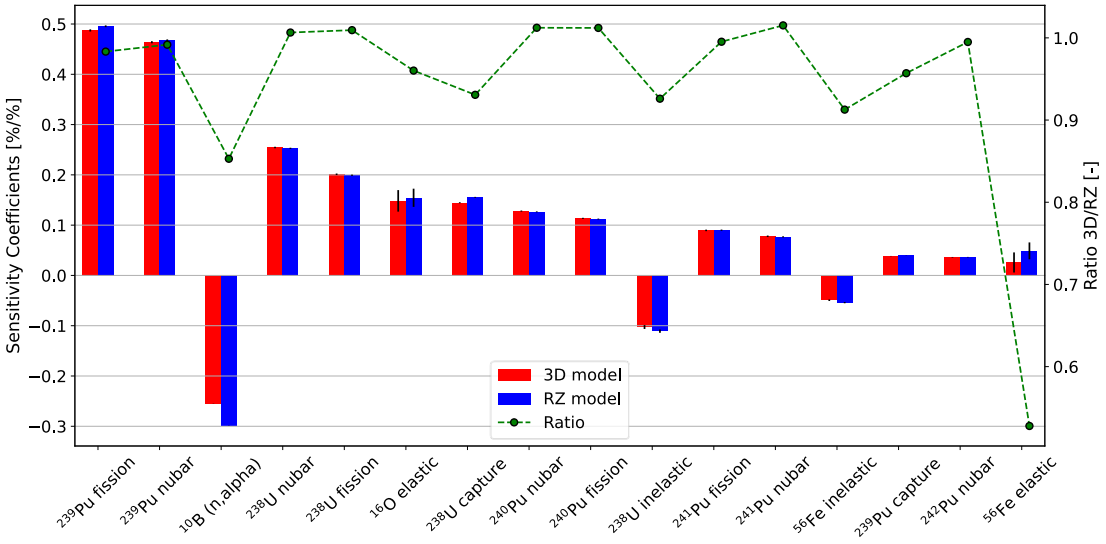

Figure A1.6. Top 16 integrated control rod worth sensitivity coefficients determined with TSUNAMI-3D CE for the heterogeneous 3D and RZ simplified models.

Sodium void has a dramatic impact on the system physics so that the proper characterization of sodium void worth is essential. Three typical sodium void scenarios are evaluated in this work: fissile region sodium void, sodium plenum void and both combined, noted as full void. For the latter one, sodium void worth sensitivities computed for both models are compared in Figure A1.7. In this case, dramatic differences can be noted when applying the simplified model. That indicates that RZ models are not adequate for sodium void worth sensitivity analyses since wrong conclusions may be extracted. Additionally, the issue related to statistical errors of scattering reactions becomes more relevant in this case. This is inherent to a Monte Carlo-based methodology and consequently reactivity coefficients analyses require a higher level of accuracy, which may be unaffordable when dealing with complex systems. In this regard, additional methodologies may be of interest for a extended intercomparison.

Total uncertainties in all the sodium void scenarios are also detailed in Table A1.7. The full void scenario presents the poorest agreement, which is consistent with observed differences on sensitivities coefficients. Additionally, relevant differences are observed in this case regarding the uncertainty breakdown (see Table A1.9). As a conclusion, RZ models do not provide high-fidelity sensitivity coefficients for reactivity responses like sodium void worth and the same behaviour is expected for other parameters such as Doppler coefficients.

Table A1.9. Detailed breakdown of uncertainty contributors for full sodium void worth using the heterogeneous 3D and RZ simplified models and 56-group SCALE6.2 covariance matrix.

Heterogeneous 3D model				Homogeneous RZ model			
	% Δρ/ρ		Std. Dev.		% Δρ/ρ		Std. Dev.
^{238}U (n,n')	21.76	±	2E-01	^{238}U (n,n')	11.98	±	9E-02
^{23}Na (n,n')	14.61	±	2E-02	^{23}Na (n,n')	10.13	±	1E-02
^{256}Fe (n,n)	9.92	±	2E-01	^{238}U (n,n')-(n,n)	4.65	±	9E-02
^{238}U (n,n')-(n,n)	9.80	±	3E-01	^{238}U (n,γ)	4.32	±	1E-03
^{238}U (n,γ)	6.64	±	2E-03	^{239}Pu (n,f)	3.22	±	1E-03

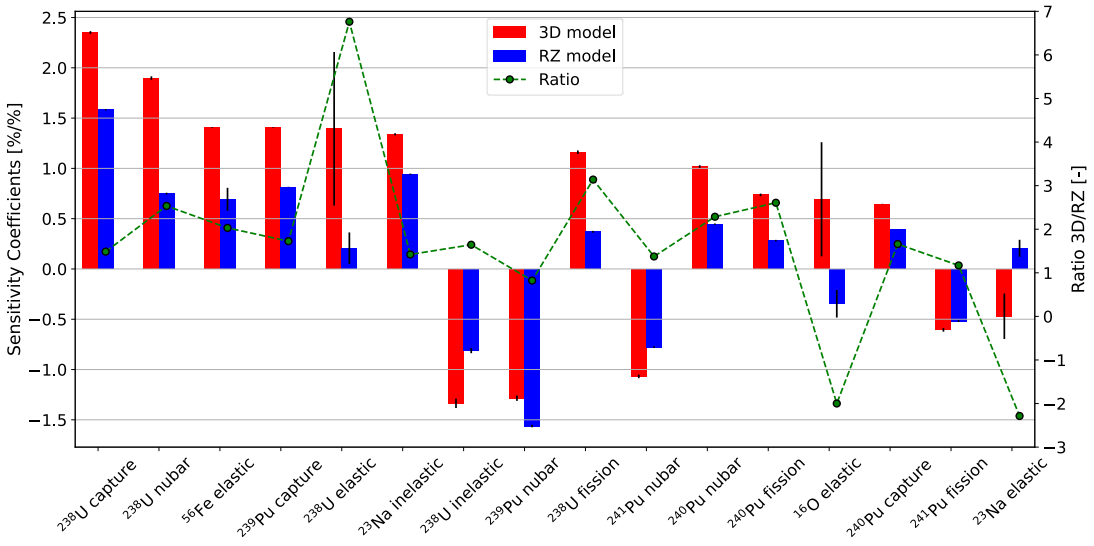

Figure A1.7. Top 16 integrated full sodium void worth sensitivity coefficients determined with TSUNAMI-3D CE for the heterogeneous 3D and RZ simplified models.

5. Discussion

Sensitivities are affected by biases arising from different nuclear data libraries, computational methods, and the assumption of modelling simplifications.

Regarding the use of different nuclear data libraries, it has been found that predicted values for the most important sensitivities are mostly independent on the evaluated library used for the transport calculations. However, differences ~7% were found for scattering reactions of ^{16}O and ^{56}Fe, even if they are accompanied with negligible statistical uncertainties. Therefore, special attention should be paid to sensitivities to scattering cross sections. The application to other advanced systems could lead to different conclusions and it is recommended to perform cross-comparison exercises, since differences in data in different evaluated libraries could lead to major differences in sensitivities.

TSUNAMI-3D CE and MG have been proven to be consistent regarding sensitivities of the multiplication factor and reactivity effects, which are not significantly affected by the self-shielding methodology. Only sensitivities to scattering cross sections exhibit significant deviations, which cannot be totally explained by the large associated statistical errors in both CE and MG methods. A comparison to deterministic-based sensitivities provided by TSUNAMI-2D is on the way aiming at analysing the scattering reactions-related issue.

Finally, it can be concluded that RZ models are suitable for multiplication factor and control rod worth sensitivity analyses, but they are not able to capture the system behaviour for reactivity responses such as sodium void worth.

Annex 2. Seven energy groups structure

Copied from M. Salvatores, "Nuclear data target accuracies: an expanded assessment, based on new covariance data and generalized methods", March 2019

The seven energy group structure results from an inspection of the energy structure of the main reactions and accounts as far as possible for some physical features of the cross-section energy shapes that could also be associated to specific experimental techniques:

- The first energy group (band) includes most of the plateau in energy of threshold fission reactions and high energy inelastic continuum
- The second band includes most discrete levels inelastic processes
- The third band includes reactions above the unresolved resonance energy range
- The fourth band represents the transition energy range between unresolved and resolved resonance ranges
- The fifth band covers the resolved resonance range
- The sixth band covers the energy range of the large actinide resonances
- The seventh band covers most of the thermal energy range

Seven energy groups structure (eV)

Group	Upper Energy
1	$1.96403\ 10^{7}$
2	$2.23130\ 10^{6}$
3	$4.97871\ 10^{5}$
4	$6.73795\ 10^{4}$
5	$2.03468\ 10^{3}$
6	$2.26033\ 10^{1}$
7	$5.40000\ 10^{-1}$

Annex 3. Uncertainty analysis of the partial voiding for the ASTRID-like reactor

A S/U analysis of six partial-voiding scenarios for ASTRID-like reactor has been performed. Each scenario represents the voiding of the coolant in a region of the core (see Figure A3.1).

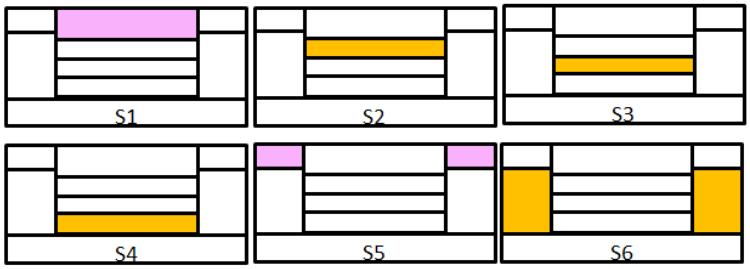

Figure A3.1. Schematic representation of the six partial-voiding scenarios. Colored regions represent the voided zones: pink illustrates sodium plenum; orange correspond to inner fuel regions (S2 and S4), inner fertile blanket (S3) and outer fuel region (S6).

Table A3.1. Major nuclide/reactions contributing to the overall relative uncertainty in sodium partial-voiding scenarios using 7g-JEFF3.3 covariance data.

Quantity	FULLVOID	S1	S2	S3	S4	S5	S6
	Δρ/ρ (%) Std. Dev.	Δρ/ρ (%) Std. Dev.	Δρ/ρ (%) Std. Dev.	Δρ/ρ (%) Std. Dev.	Δρ/ρ (%) Std. Dev.	Δρ/ρ (%) Std. Dev.	Δρ/ρ (%) Std. Dev.
^{239}Pu (n,f)	11.5 ± 5E-03	0.5 ± 6E-04	4.4 ± 7E-03	3.3 ± 9E-03	4.4 ± 1E-02	0.5 ± 2E-03	7.4 ± 2E-02
^{239}Pu (n,γ)	6.3 ± 3E-03		2.5 ± 4E-03	1.7 ± 5E-03	2.4 ± 8E-03		4.1 ± 9E-03
^{238}U (n,n')	6.1 ± 6E-02	0.6 ± 2E-02	1.5 ± 5E-02	1.8 ± 9E-02	2.2 ± 1E-01	0.9 ± 1E-01	2.7 ± 1E-01
^{238}U (n,n') (n,f)	-4.5 ± 2E-02	-0.7 ± 1E-02			-1.0 ± 2E-02	-0.8 ± 5E-02	-2.9 ± 3E-03
^{239}Pu (n,f) (n, γ)	-4.4 ± 9E-04		-1.7 ± 1E-03	-1.2 ± 1E-03	-1.7 ± 2E-03		
^{238}U (n,γ)	3.8 ± 1E-03		1.4 ± 2E-03	1.4 ± 3E-03	1.4 ± 4E-03		2.5 ± 4E-03
^{23}Na (n,γ)	3.7 ± 2E-04		1.4 ± 3E-04	1.0 ± 4E-04	1.4 ± 6E-04		2.4 ± 7E-04
^{240}Pu (n,f)	3.2 ± 2E-03	0.7 ± 8E-04				0.7 ± 4E-03	
^{56}Fe el.	3.1 ± 4E-02	0.9 ± 3E-02				0.9 ± 1E-01	2.7 ± 1E-01
^{238}U el. (n,n')	-3.1 ± 2E-02	-0.5 ± 9E-03				-0.6 ± 5E-02	
^{241}Pu (n,f)	2.7 ± 4E-04		1.1 ± 5E-04		1.1 ± 1E-03		1.8 ± 1E-03
^{238}U (n,f)	2.5 ± 1E-03	0.6 ± 7E-04				0.6 ± 3E-03	
^{240}Pu (n,f) (n, γ)	2.4 ± 1E-03						
^{238}U (n,f) (n, γ)	2.3 ± 9E-04						
^{238}U (n,n') (n,γ)	-2.2 ± 2E-02		-1.1 ± 2E-02				-1.9 ± 5E-02
^{56}Fe (n,γ)	2.2 ± 8E-04			0.6 ± 1E-03			
^{23}Na (n,n')	2.1 ± 1E-03		1.1 ± 2E-03	0.6 ± 2E-03	1.0 ± 4E-03		1.6 ± 4E-03
^{238}U el. (n,f)	2.0 ± 9E-03	0.5 ± 6E-03				0.5 ± 3E-02	
^{239}Pu χ	1.9 ± 7E-04	0.7 ± 7E-04				0.8 ± 4E-03	
^{23}Na el.	1.7 ± 1E-02	1.3 ± 2E-02	1.9 ± 5E-02	1.6 ± 7E-02	1.1 ± 7E-02	1.3 ± 1E-01	
TOTAL LISTED	**15.71 (97%)**	**2.0 (88%)**	**5.8 (94%)**	**4.7 (95%)**	**5.8 (94%)**	**2.0 (84%)**	**9.6 (95%)**
OVERALL	**16.2 ± 8E-02**	**2.3 ± 5E-02**	**6.2 ± 8E-02**	**4.9 ± 1E-01**	**6.2 ± 2E-01**	**2.4 ± 3E-01**	**10.1 ± 2E-01**

With the goal of illustrating the flux anisotropy in SFR, Figures A3.2 and A3.3 show the most relevant flux moments in the sodium plenum regions for ASTRID-like reactor in two situations: no voiding and voiding respectively. In sodium plenum regions (SPL), the flux moment 1 is only one order of magnitude smaller than the scalar flux. The anisotropic scattering reactions in the sodium plenum causes the flux to be anisotropic in this region. In case of voiding, the flux moments are much higher and even third-order flux moments (from flux moment 9 on) become relevant.

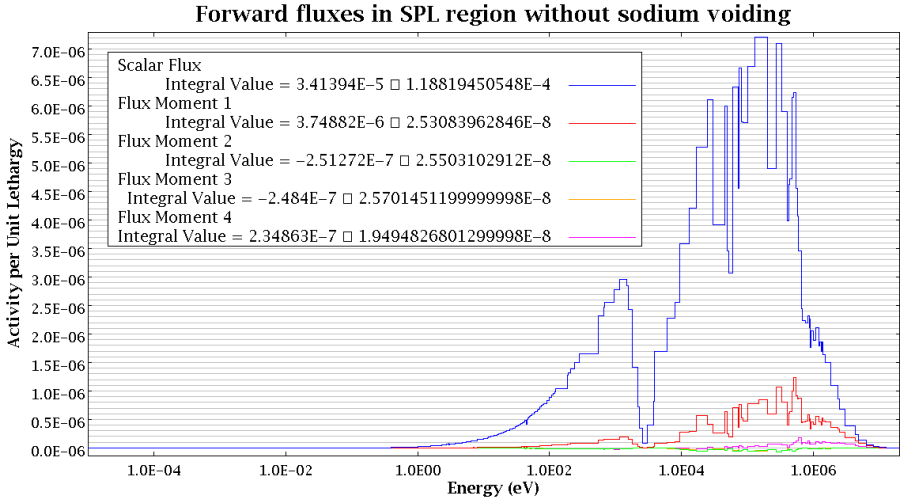

Figure A3.2. Forward flux moments in sodium plenum

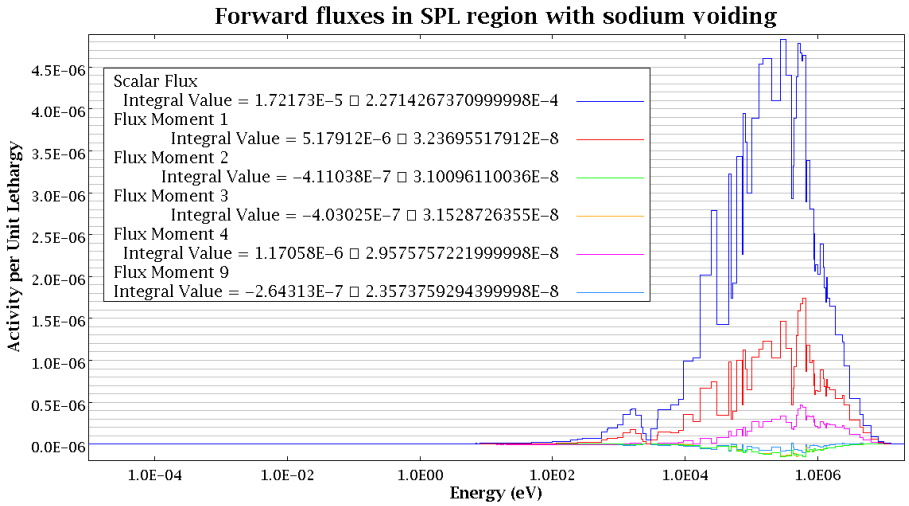

Figure A3.3. Forward flux moments in voided sodium plenum

Annex 4. Sensitivity profiles of critical cross sections

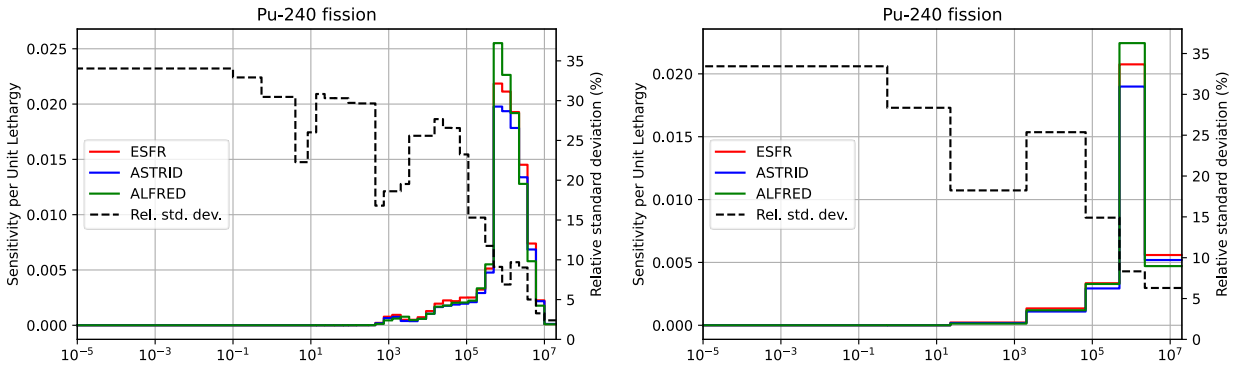

Figure A4.1. 33- and 7-group multiplication factor sensitivity profiles of ^{240}Pu (n,f) for ESFR, ASTRID and ALFRED designs along with the uncertainty of the quantity in the JEFF-3.3 AMPX-formatted covariance matrix.

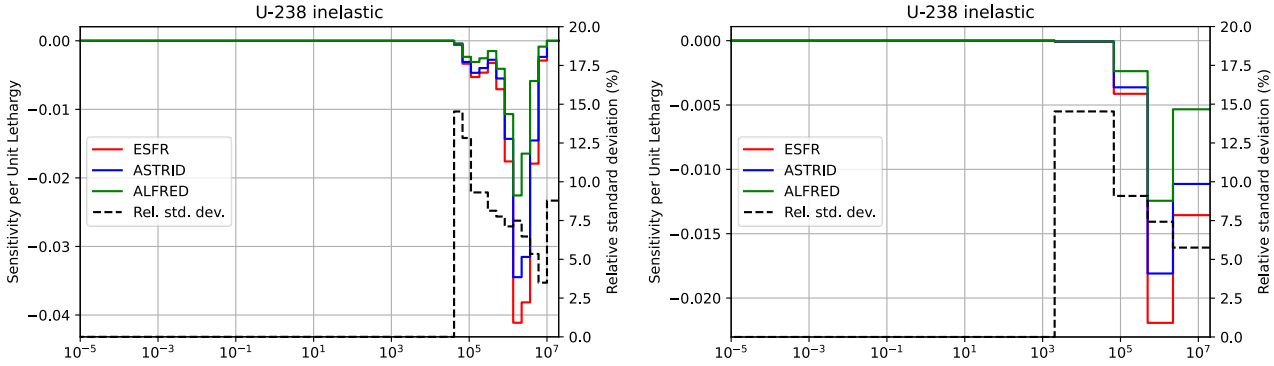

Figure A4.2. 33- and 7-group multiplication factor sensitivity profiles of ^{238}U (n,n') for ESFR, ASTRID and ALFRED designs along with the uncertainty of the quantity in the JEFF-3.3 AMPX-formatted covariance matrix.

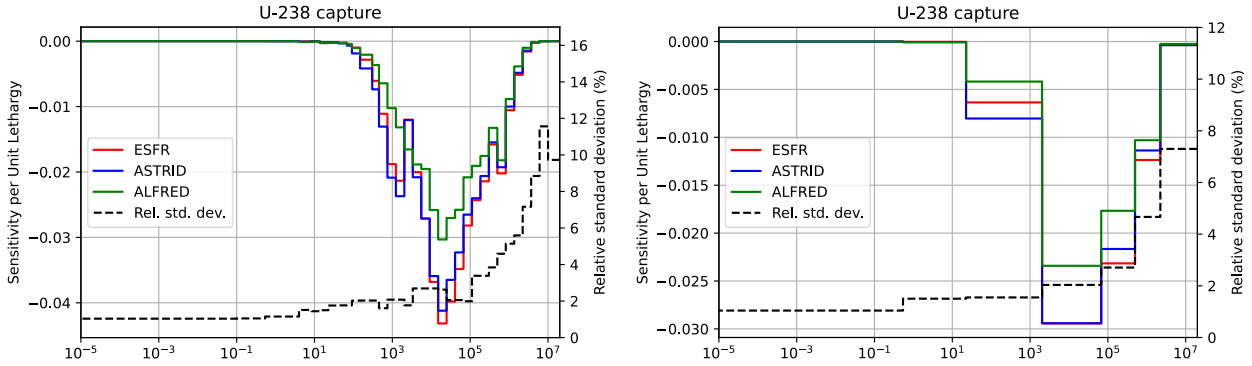

Figure A4.3. 33- and 7-group multiplication factor sensitivity profiles of ^{238}U (n,γ) for ESFR, ASTRID and ALFRED designs along with the uncertainty of the quantity in the JEFF-3.3 AMPX-formatted covariance matrix.

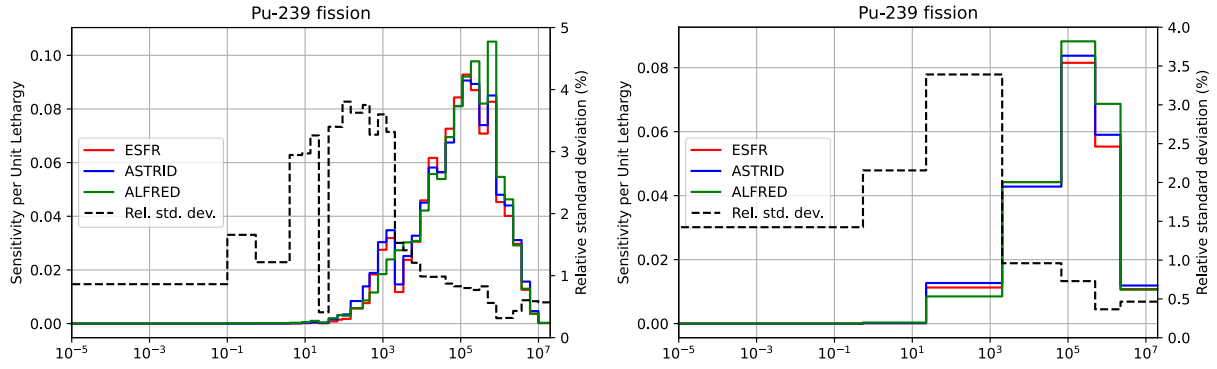

Figure A4.4. 33- and 7-group multiplication factor sensitivity profiles of ^{239}Pu (n,f) for ESFR, ASTRID and ALFRED designs along with the uncertainty of the quantity in the JEFF-3.3 AMPX-formatted covariance matrix.

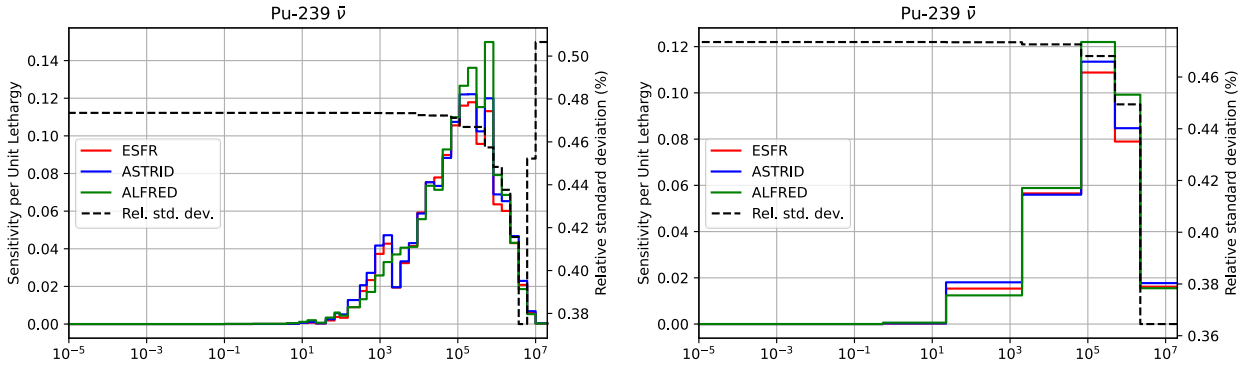

Figure A4.5. 33- and 7-group multiplication factor sensitivity profiles of ^{239}Pu ν for ESFR, ASTRID and ALFRED designs along with the uncertainty of the quantity in the JEFF-3.3 AMPX-formatted covariance matrix.

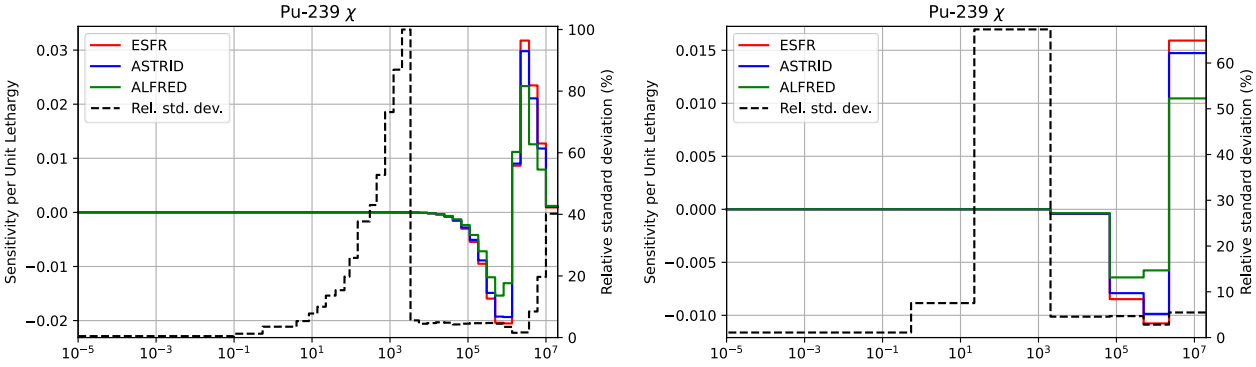

Figure A4.6. 33- and 7-group multiplication factor sensitivity profiles of ^{239}Pu χ for ESFR, ASTRID and ALFRED designs along with the uncertainty of the quantity in the JEFF-3.3 AMPX-formatted covariance matrix.

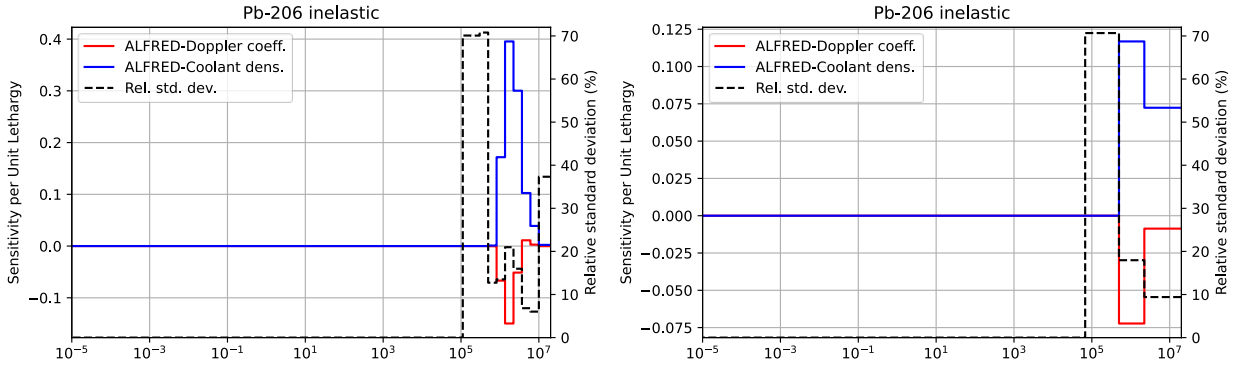

Figure A4.7. 33- and 7-group Doppler and coolant density coefficients sensitivity profiles of ^{206}Pb (n,n') for ALFRED design along with the uncertainty of the quantity in the JEFF-3.3 AMPX-formatted covariance matrix.

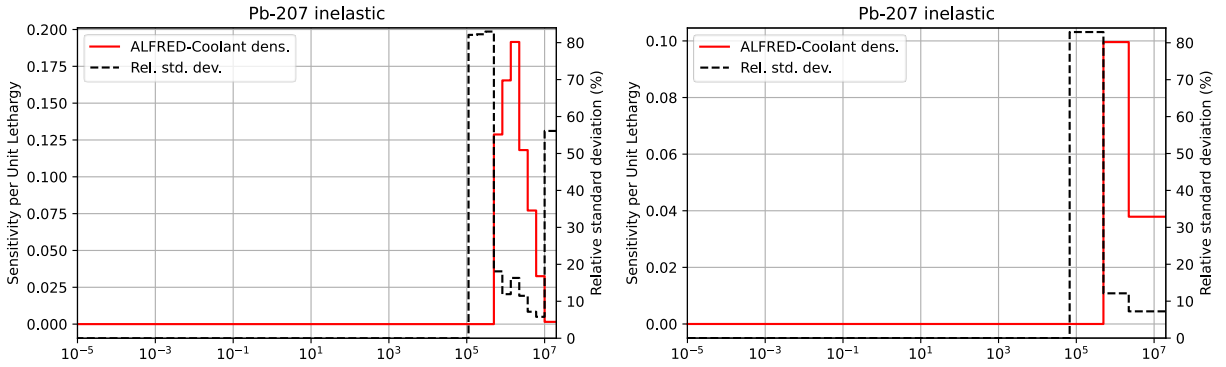

Figure A4.8. 33- and 7-group coolant density coefficient sensitivity profiles of ^{207}Pb (n,n') for ALFRED design along with the uncertainty of the quantity in the JEFF-3.3 AMPX-formatted covariance matrix.

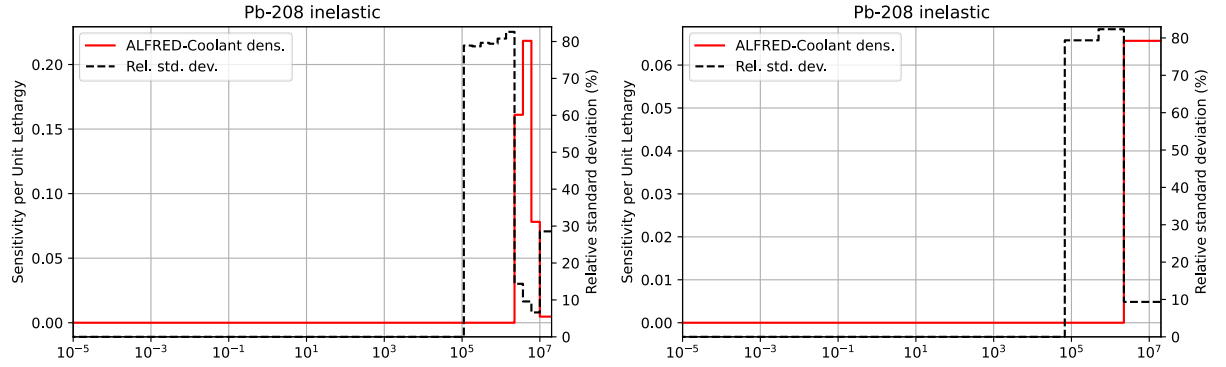

Figure A4.9. 33- and 7-group coolant density coefficient sensitivity profiles of ^{208}Pb (n,n') for ALFRED design along with the uncertainty of the quantity in the JEFF-3.3 AMPX-formatted covariance matrix.

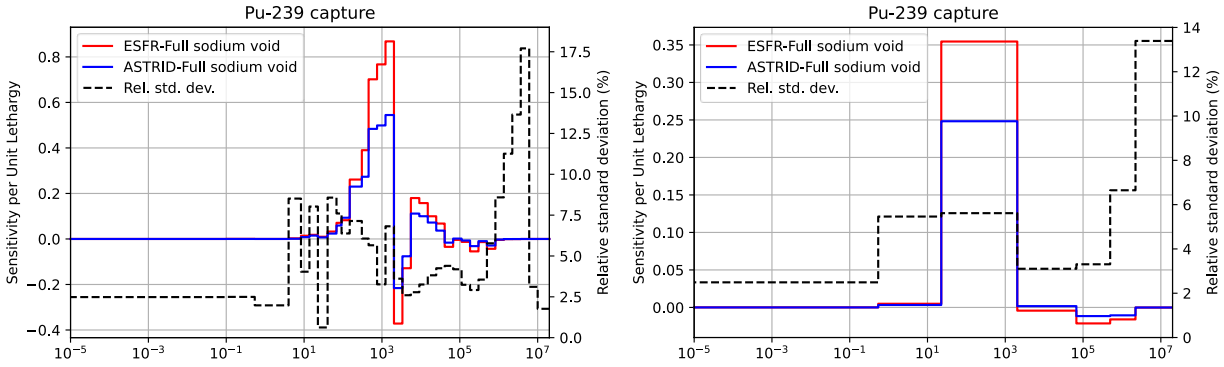

Figure A4.10. 33- and 7-group full sodium void coefficient sensitivity profiles of ^{239}Pu (n,γ) for ESFR and ASTRID along with the uncertainty of the quantity in the JEFF-3.3 AMPX-formatted covariance matrix.

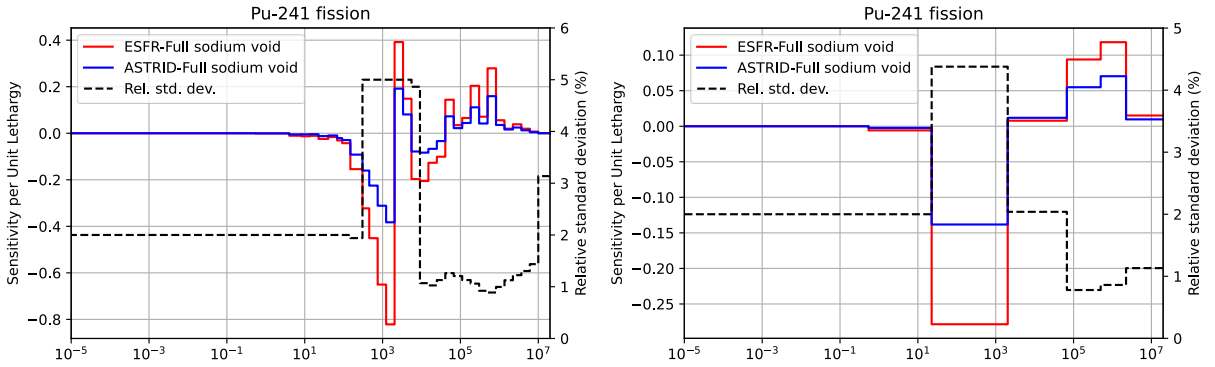

Figure A4.11. 33- and 7-group full sodium void coefficient sensitivity profiles of ^{241}Pu (n,f) for ESFR and ASTRID along with the uncertainty of the quantity in the JEFF-3.3 AMPX-formatted covariance matrix.

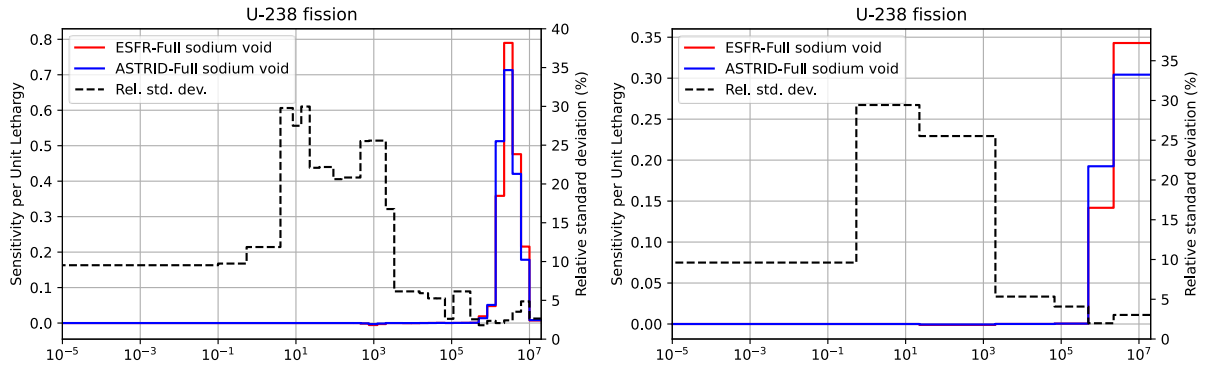

Figure A4.12. 33- and 7-group full sodium void coefficient sensitivity profiles of ^{238}U (n,f) for ESFR and ASTRID along with the uncertainty of the quantity in the JEFF-3.3 AMPX-formatted covariance matrix.

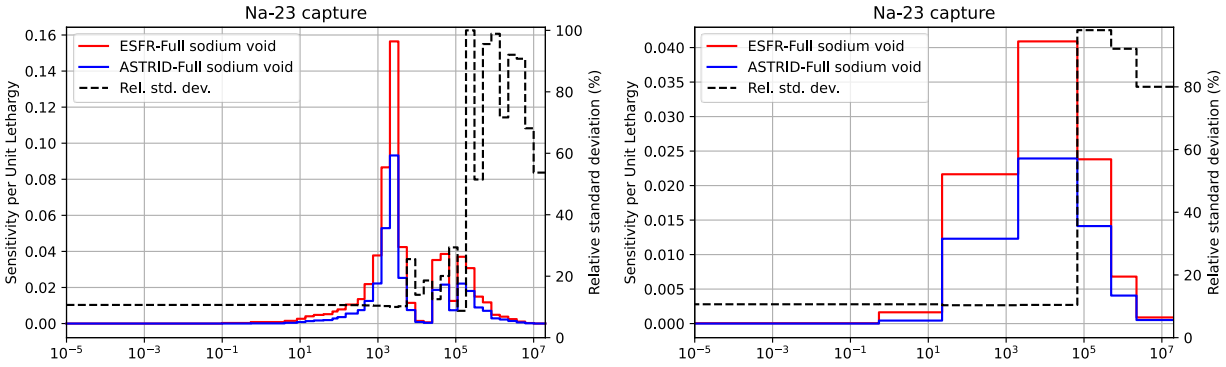

Figure A4.13. 33- and 7-group full sodium void coefficient sensitivity profiles of ^{23}Na (n,γ) for ESFR and ASTRID along with the uncertainty of the quantity in the JEFF-3.3 AMPX-formatted covariance matrix.

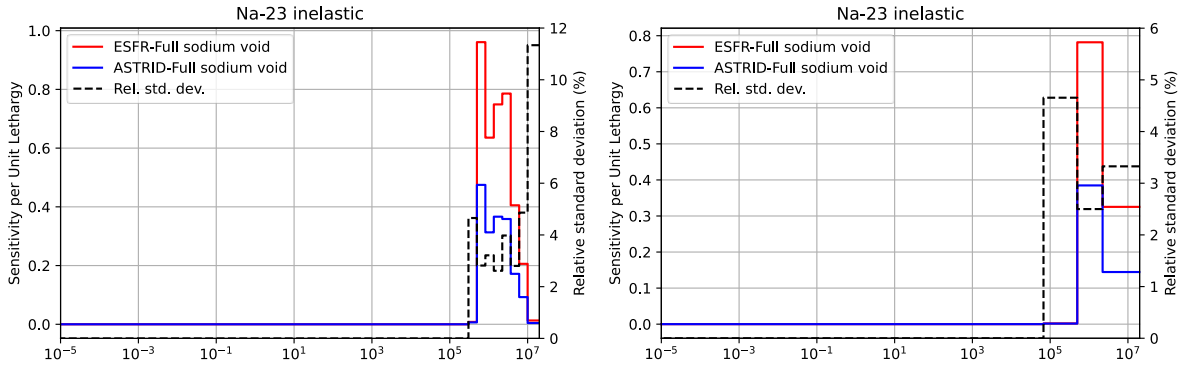

Figure A4.14. 33- and 7-group full sodium void coefficient sensitivity profiles of ^{23}Na (n,n') for ESFR and ASTRID along with the uncertainty of the quantity in the JEFF-3.3 AMPX-formatted covariance matrix.

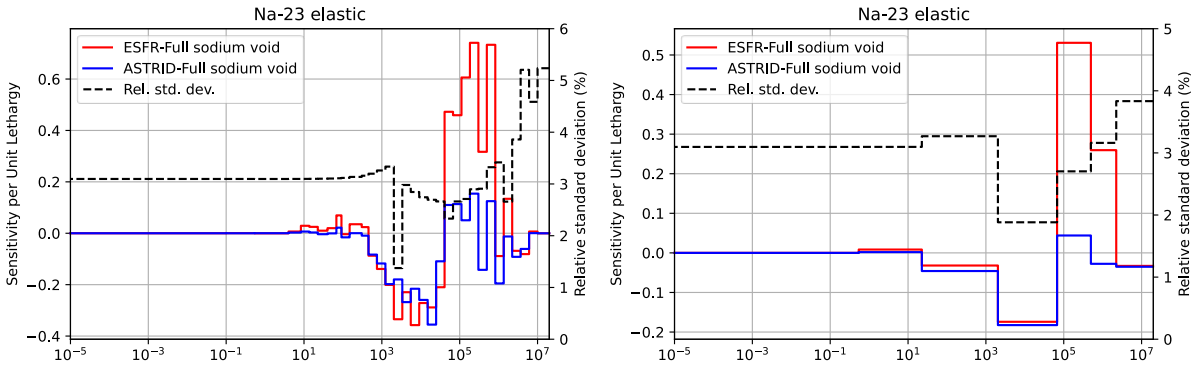

Figure A4.15. 33- and 7-group full sodium void coefficient sensitivity profiles of ^{23}Na (n,n) for ESFR and ASTRID along with the uncertainty of the quantity in the JEFF-3.3 AMPX-formatted covariance matrix.

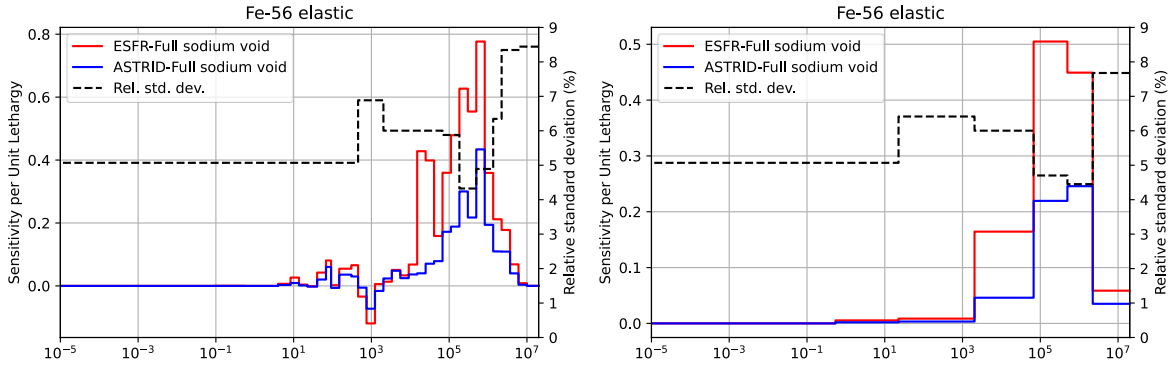

Figure A4.16. 33- and 7-group full sodium void coefficient sensitivity profiles of ^{56}Fe (n,n) for ESFR and ASTRID along with the uncertainty of the quantity in the JEFF-3.3 AMPX-formatted covariance matrix.

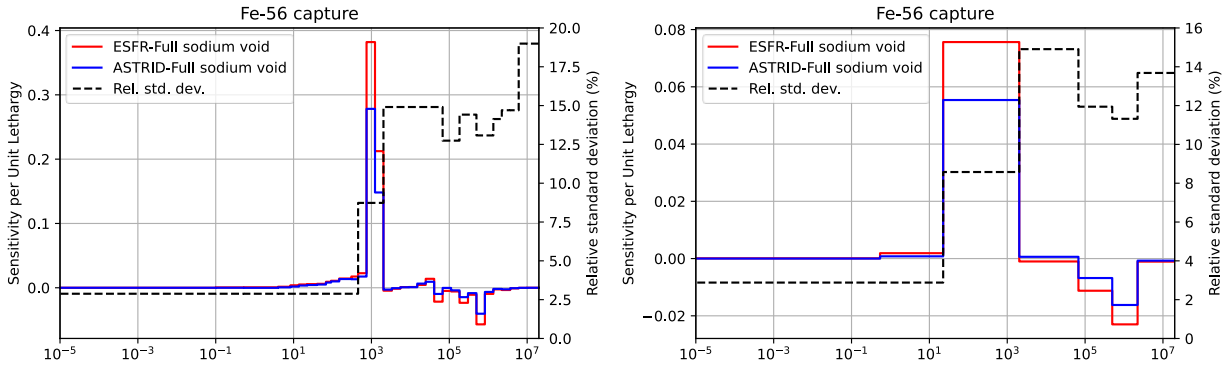

Figure A4.17. 33- and 7-group full sodium void coefficient sensitivity profiles of ^{56}Fe (n,γ) for ESFR and ASTRID along with the uncertainty of the quantity in the JEFF-3.3 AMPX-formatted covariance matrix.